

Dysregulated mitophagy and mitochondrial organization in optic atrophy due to *OPA1* mutations

OPEN

Chunyan Liao, PhD
Neil Ashley, PhD
Alan Diot, PhD
Karl Morten, PhD
Kanchan Phadwal, PhD
Andrew Williams, MD
Ian Fearnley, MD
Lyndon Rosser, BSc
Jo Lowndes, MSc, BSc
Carl Fratter, BA
David J.P. Ferguson,
PhD, DSc
Laura Vay, PhD
Gerardine Quaghebeur,
MD
Isabella Moroni, MD
Stefania Bianchi, MD
Costanza Lamperti, MD,
PhD
Susan M. Downes, MD
Kamil S. Sitarz, PhD
Padraig J. Flannery, BA,
MSc
Janet Carver, MSc
Eszter Dombi, BSc
Daniel East, PhD
Matilde Laura, PhD
Mary M. Reilly, MD
Heather Mortiboys, PhD
Remko Prevo, PhD
Michelangelo
Campanella, PhD
Matthew J. Daniels, PhD,
MRCP
Massimo Zeviani, MD
Patrick Yu-Wai-Man,
PhD, FRCOphth
Anna Katharina Simon,
PhD
Marcela Votruba, PhD,
FRCOphth
Joanna Poulton, DM

ABSTRACT

Objective: To investigate mitophagy in 5 patients with severe dominantly inherited optic atrophy (DOA), caused by depletion of *OPA1* (a protein that is essential for mitochondrial fusion), compared with healthy controls.

Methods: Patients with severe DOA (DOA plus) had peripheral neuropathy, cognitive regression, and epilepsy in addition to loss of vision. We quantified mitophagy in dermal fibroblasts, using 2 high throughput imaging systems, by visualizing colocalization of mitochondrial fragments with engulfing autophagosomes.

Results: Fibroblasts from 3 biallelic *OPA1*(-/-) patients with severe DOA had increased mitochondrial fragmentation and mitochondrial DNA (mtDNA)-depleted cells due to decreased levels of *OPA1* protein. Similarly, in siRNA-treated control fibroblasts, profound *OPA1* knockdown caused mitochondrial fragmentation, loss of mtDNA, impaired mitochondrial function, and mitochondrial mislocalization. Compared to controls, basal mitophagy (abundance of autophagosomes colocalizing with mitochondria) was increased in (1) biallelic patients, (2) monoallelic patients with DOA plus, and (3) *OPA1* siRNA-treated control cultures. Mitophagic flux was also increased. Genetic knockdown of the mitophagy protein ATG7 confirmed this by eliminating differences between patient and control fibroblasts.

Conclusions: We demonstrated increased mitophagy and excessive mitochondrial fragmentation in primary human cultures associated with DOA plus due to biallelic *OPA1* mutations. We previously found that increased mitophagy (mitochondrial recycling) was associated with visual loss in another mitochondrial optic neuropathy, Leber hereditary optic neuropathy (LHON). Combined with our LHON findings, this implicates excessive mitochondrial fragmentation, dysregulated mitophagy, and impaired response to energetic stress in the pathogenesis of mitochondrial optic neuropathies, potentially linked with mitochondrial mislocalization and mtDNA depletion.

Neurology® 2017;88:1-12

GLOSSARY

DOA = dominantly inherited optic atrophy; **IMM** = inner mitochondrial membrane; **LC3** = light chain 3; **LHON** = Leber hereditary optic neuropathy; **MMP** = mitochondrial membrane potential; **mtDNA** = mitochondrial DNA; **MFN2** = mitofusin 2; **MTOC** = microtubule-organizing center; **PINK1** = PTEN-induced putative kinase 1; **TMRM** = tetramethyl rhodamine methyl ester.

Autosomal dominant optic atrophy (DOA) is the commonest autosomal form of mitochondrial optic neuropathy, with most patients harboring pathogenic mutations in the optic atrophy 1 (*OPA1*) gene. *OPA1* mutations cause dominantly inherited progressive visual failure in the first 2 decades, secondary to optic nerve neurodegeneration. Strikingly, a subgroup of patients develops a multisystemic neurologic phenotype, known as DOA plus. Other obligate *OPA1* mutation carriers are visually asymptomatic. The mode of inheritance is autosomal dominant in the majority of cases, either haploinsufficiency or dominant-negative, with DOA plus patients frequently harboring missense mutations in the GTPase domain.

Author affiliations are provided at the end of the article.

Go to Neurology.org for full disclosures. Funding information and disclosures deemed relevant by the authors, if any, are provided at the end of the article. The Article Processing Charge was paid by the Wellcome Trust and Charity Open Access Fund.

This is an open access article distributed under the terms of the Creative Commons Attribution License 4.0 (CC BY), which permits unrestricted use, distribution, and reproduction in any medium, provided the original work is properly cited.

OPA1 appears to regulate mitochondrial quality control mediated through mitophagy,¹ a specialized type of autophagy.² Mitophagy is one among several types of mitochondrial quality control,³ and the only pathway known to turn over whole mitochondrial genomes. It is crucial for normal development⁴ and allows dysfunctional mitochondrial DNA (mtDNA) to be recycled instead of triggering cell death.⁵

We previously demonstrated increased mitophagy in fibroblasts from patients with Leber hereditary optic neuropathy (LHON).⁶ This was attenuated by idebenone, which conferred symptomatic improvement.⁶ To clarify whether increased mitophagy is an important feature of mitochondrial optic neuropathies, we investigated the role of *OPA1* in mitophagy in primary *OPA1* mutant fibroblasts from 5 patients in 3 families with severe DOA plus phenotypes. We also studied the effects of siRNA-mediated knockdown of *OPA1* in primary human control fibroblasts. Because *OPA1* deficiency is widely expressed, fibroblasts have been extensively used to model the cellular mechanisms occurring in retinal ganglion and muscle cells in this multisystem disease.^{7,8}

METHODS Mitophagy is a sequence of events in which a structure known as the autophagosome⁹ forms and engulfs spent mitochondria in a process facilitated by microtubule motors. The autophagosome is then transported towards the cellular microtubule-organizing center¹⁰ (MTOC) and fuses with lysosomes, ultimately resulting in the degradation of its enclosed cargo. We therefore quantified mitophagy by counting autophagosomes, that is, characteristic puncta positive for microtubule-associated protein 1 light chain 3 (LC3), and colocalizing with mitochondrial markers.²

Standard protocol approvals, registrations, and patient consents. *Ethics: Patient and control fibroblast lines.* Patient and control samples were obtained with informed consent with the approval of the UK National Research Ethics Service (South Central-Berkshire and Newcastle and North Tyneside), or of the Ethical Committee of the Fondazione Carlo Besta Institute of Neurology, according to the Declaration of Helsinki. Donors included 5 patients with DOA plus phenotypes, 5 other family members sharing mutant *OPA1* alleles, and 20 normal controls.

Pedigrees of 3 biallelic patients harboring compound heterozygous *OPA1* mutations (strictly described as semi-dominant^{11–13}) are presented in figure 1A. A summary of the clinical presentations and genotypes of all patients (illustrated in figure 1B) are presented in the table. This includes chronic progressive external ophthalmoplegia with an apparent defect in mtDNA maintenance^{14,15} that remains unexplained (DOA plus *OPA1*[+/-]1 and 2, table). Further details of the clinical presentation, a cranial MRI scan of the biallelic patients, and the likely effects on protein are presented in appendix e-1 and figure e-1, A and B, at

Neurology.org. Following the convention of previous authors,¹³ we designated the 3 biallelic patients DOA plus because each had clinical and electrophysiologic evidence of both peripheral and optic neuropathy.

Immunofluorescence and live cell imaging. Cells were processed for histochemistry, immunofluorescence, or live staining with PicoGreen and tetramethyl rhodamine methyl ester (TMRM) as previously described (appendix e-2). We used 2 high-throughput imaging systems for detecting mitophagy: the established IN Cell 1000¹⁶ and ImageStream, which we validated (figure e-2).

Statistical analysis. Statistical analysis is detailed in appendix e-2.

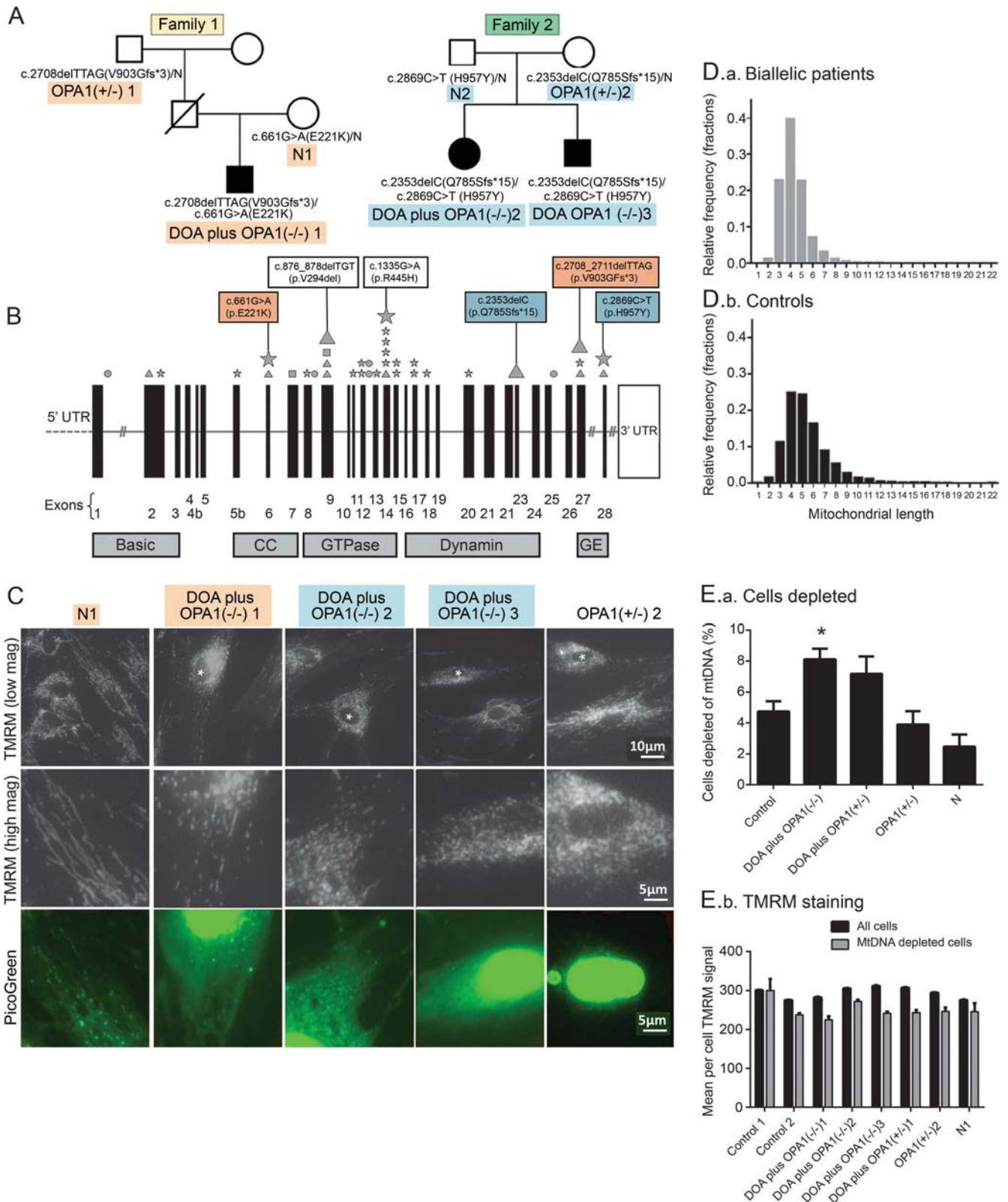
RESULTS Biallelic *OPA1* mutant patients and families.

We studied primary fibroblasts, carrying biallelic *OPA1* mutations, from patients and transmitting relatives belonging to 2 families (see table for an explanation of nomenclature, figure 1A for pedigree, and appendix e-1 for additional clinical details). The proband of family 1, DOA plus *OPA1*(-/-)1, is a 17-year-old boy presenting with a severe *OPA1* phenotype (figure 1A). DOA plus *OPA1*(-/-)1 carries a c.2708_2711delTTAG p.V903Gfs*3 mutation, found in the paternal grandfather, in trans with a maternal c.661G>A p.E221K change (*OPA1*[+/-]1 and N1, respectively, in figure 1A). In family 2, biallelic patients DOA plus *OPA1*(-/-)2 and 3 both had a paternal c.2353delC p.Q785Sfs*15 and a maternal c.2869C>T, p.H957Y mutation (figure 1, A and B; see figure e-1B for PolyPhen analysis). No other relatives were affected. The frameshift mutation in family 1 is a well-established pathogenic mutation.¹⁷ None of these mutations involves the GTPase domain of *OPA1*, classically implicated in syndromic DOA,¹³ examples of which were identified in monoallelic DOA plus families 3 and 4 (table).

Fibroblasts from DOA plus patients have a fragmented mitochondrial network with occasional mtDNA-depleted cells.

We investigated the cellular phenotype of probands, transmitting relatives, and controls. We visualized both mtDNA and mitochondria by using the DNA-specific dye PicoGreen and the mitochondrial membrane potential (MMP)-sensitive dye TMRM.¹⁸ The mitochondrial network had a fragmented morphology in a small minority of cells from patients DOA plus *OPA1*(-/-)1–3, but it was normal in other cells (figure 1C). Using high-throughput imaging (figure 1D), we showed that mitochondria in fibroblasts from biallelic and monoallelic DOA plus patients (DOA plus *OPA1*[-/-]1–3 and DOA plus *OPA1*[+/-]1–2) were significantly more fragmented than mitochondria from 6 controls ($p = 0.005$ and 0.01 , respectively, figure e-3A). Using PicoGreen to visualize mtDNA,¹⁹ we found a significant increase in cells that were

Figure 1 Genetic analysis of a family with a very severe dominantly inherited optic atrophy (DOA) plus phenotype



(A) Pedigrees of families 1 and 2. (B) *OPA1* gene structure. Diagrammatic representation of the *OPA1* gene. The diagram indicates the location both of mutations resulting in DOA plus syndromes as described⁸ (small symbols) and of the mutations reported in this study (large symbols; highlighting corresponds to pedigree). Mutation type: stars (missense); squares (nonsense); circles (splice site); triangles (deletion). CC = coiled-coil domain; GE = GTPase effector domain; UTR = untranslated region. (C) PicoGreen/tetramethyl rhodamine methyl ester (TMRM) costaining of live fibroblasts from biallelic DOA plus *OPA1(-/-)*-1-3 patients, and their symptom-free mothers (N1 and *OPA1(+/-)*-2; see A). PicoGreen stains DNA and TMRM is sensitive to mitochondrial

Continued

depleted of mtDNA in biallelic patients compared to controls with IN Cell 1000 ($p < 0.001$, figure 1E). In all cultures, these mtDNA-depleted cells had fragmented mitochondria with a lower membrane potential (figure 1E.a and 1E.b) than control cells. Intermediate mitochondrial fragmentation and mtDNA depletion were present in fibroblast cultures from DOA *OPA1*(+/-) but not from non-syndromic DOA (figure e-3A) or the asymptomatic, obligate carrier relatives of the biallelic patients.

***OPA1* knockdown causes mtDNA depletion and alters the distribution of mitochondria in control cells.** To determine whether mitochondrial DNA depletion is a consistent effect of *OPA1* knockdown²⁰ and whether it would be sufficient to affect mitochondrial function, we then knocked down *OPA1* in control fibroblasts using a pan-*OPA1*-specific siRNA,²¹ thus modeling the reduction in full-length *OPA1* protein in patient cells. Compared to the reduced *OPA1* protein levels seen in the patient fibroblasts, the siRNA achieved a more profound reduction (figure 2A), and knockdown cells underwent fragmentation and perinuclear clustering of the mitochondrial network (figure 2B).

Next, we visualized both mtDNA and mitochondria in the *OPA1* siRNA-treated cells,¹⁸ and found a marked loss of mtDNA (figure 2C). In these cells, mitochondria clustered in the perinuclear region (figure 2, B–D), and often displayed high TMRM fluorescence, suggesting increased MMP or increased organelle density. We confirmed these findings using anti-DNA immunoglobulin M/MitoTracker colabeling of mtDNA (figure 2C) and real-time PCR (figure 2E). Despite the considerable mtDNA depletion, COX activity was largely preserved at 5 days, but reduced by 14 days (figure 2D).

By using an antibody against pericentrin, we showed that the perinuclear mitochondrial clusters consistently colocalized with the MTOC (figure 2F.a). As well as being crucial for neuronal survival and function, microtubule-dependent transport mediates efficient encounters of autophagosomes with lysosomes,²² which cluster near the nucleus under conditions such as nutrient deprivation.^{15,23} A similar clustering of mitochondria occurs by overexpressing

tau,²⁴ because tau inhibits microtubule-dependent plus-end-directed transport of mitochondria. Thus, we hypothesized that clustering of mitochondria at the MTOC in knockdown cells may be due to either decreased plus-end or increased minus-end transport caused by excessive fragmentation and mitophagy. To test this idea, we exposed cells to microtubule-disrupting drugs. Nocodazole, which disassembles microtubules, rescued the perinuclear clustering so that the distribution of mitochondria resembled that in control cells (figure 2F.b). Exposure to taxotere (disrupts MTOC) and cytochalasin D (depolymerizes actin) disrupted perinuclear mitochondrial clustering, supporting our assertion that it depends on microtubules and MTOC. For a more detailed explanation, see figure e-3B. Together, these results demonstrate that *OPA1* knockdown in primary human fibroblasts causes disruption of the mitochondrial network, partial mtDNA depletion, and microtubule-dependent rearrangement of the mitochondrial distribution.

High-throughput imaging shows that patient fibroblasts harbor increased autophagosomes colocalizing with mitochondria compared to controls. We reasoned that the depletion of mtDNA associated with *OPA1* knockdown could be due either to slowed mtDNA synthesis or to increased mtDNA turnover and therefore investigated whether *OPA1* insufficiency/dysfunction had affected mitophagy. We measured total mitochondrial autophagy irrespective of *Parkin* and *PINK1* using 2 high-throughput imaging systems, ImageStream and IN Cell 1000,¹⁶ which are established methods for quantifying autophagy and mitophagy. In each of these, antibodies to LC3 and Tom20 are used to immunolabel autophagosomes and mitochondria, respectively. In figure e-2D, we show that ImageStream and IN Cell 1000 techniques are comparable.

Fibroblasts from DOA plus *OPA1*(-/-)2 and 3 (figure 3A.a) and DOA plus *OPA1*(-/-)1 (figure 3A.b and 3A.c) patients all harbored significantly more LC3-positive puncta colocalizing with mitochondrial fragments, and hence more mitophagy than those from the control using ImageStream. Colocalization of the lysosomal marker, LyosID, with LC3 puncta is used to demonstrate autolysosomes, a later stage of mitophagy than autophagosomes (figure 3A.a

Figure 1 legend, continued:

membrane potential. Nuclei of cells exhibiting mitochondrial fragmentation are marked with an asterisk. PicoGreen panel shows the same field as the high-magnification TMRM panel. TMRM staining of cells from biallelic DOA plus patients with abnormal mitochondrial fragmentation were often also depleted of mtDNA (E), but this was more marked in the siRNA-treated cell cultures in figure 2. (D) We used IN Cell 1000 to measure the mean mitochondrial length in fibroblast cultures, stained either with TMRM and PicoGreen^{25,26} or with antibody to mitochondrial protein Tom20. Cultures were grown for 3 days in 96-well plates in triplicate. To quantify the degree of mitochondrial fragmentation, we measured the average mitochondrial length in each cell and plotted a frequency distribution. This shows that while the modal length was similar in both groups, the per cell average mitochondrial length was shorter in biallelic patients (D.a) than controls (D.b) (see also figure e-3). (E) Cells depleted of mtDNA are increased (E.a) and have a lower membrane potential by TMRM staining (E.b). Error bars are 1 standard error. Asterisks indicate $p < 0.001$ compared to controls (2-tailed t test). Each bar represents between 400 and 1,500 cells. mtDNA = mitochondrial DNA.

Table Clinical details of 4 families studied

Family	Mutation	Current age, y	Sex	Onset, y	Left eye	Right eye	Optic atrophy	Ataxia	Myopathy	Peripheral neuropathy	Spasticity	Cognitive impairment	Other	Designation for this article
1	c.2708_2711delTTAG/ c.661G>A	17	M	2	CF	HM	Y	Y	N	Y	Y	Y	Migraine, epilepsy	DOA plus, <i>OPA1</i> (-/-)1
					NA	NA	N	N	N	N		<i>OPA1</i> (+/-)1		
					6/5	6/6	N	N	N	N		N1		
2	c.2353delC/ c.2869C>T	12	F	3	1/10	1/20	Y	N	N	Y	N		DOA plus, <i>OPA1</i> (-/-)2	
				2	1/20	1/20	Y	N	N	N		DOA plus, <i>OPA1</i> (-/-)3		
3	c.2869C>T/N c.2353delC/N c.876_878delTGT/N	47	M	NA	N	N	N	N	N	N	N	N		N2
				41	N	N	Y	N	N	N	N		<i>OPA1</i> (+/-)2	
				5	CF	CF	Y	N	Y	Y	Migraine	DOA plus, <i>OPA1</i> (+/-)1		
4	c.876_878delTGT/N c.1334G>A/N	31	M	11	20/40	20/60	Y	N	N	N	N		DOA, <i>OPA1</i> (+/-)	
				20	NA	NA	Y	N	N	N		DOA plus, <i>OPA1</i> (+/-)2		

Abbreviations: + = wild-type; - = an established or a likely pathogenic mutation; CF = counting fingers, i.e., poor visual function; HM = hand movements only, very poor visual function; N = normal; NA = not available.

Patients are numbered by their *OPA1* genotype, *OPA1*(-/-) being biallelic, *OPA1*(+/-) being monoallelic. Phenotype is indicated as DOA for patients who have visual failure but no additional neurologic features, and DOA plus as patients manifesting extraocular neurologic manifestations in addition to visual failure, as part of an expanded dominant optic atrophy plus phenotype. N1 and N2 (normal) individuals carry only a novel missense *OPA1* mutation. Missense mutations c.661G>A (p.E221K) and c.1334G>A (p.R445H) are novel and absent from >450 chromosomes from DOA patients and >13,000 alleles (ensemble linked to dbSNP); we surmise they are neither common causes of optic nerve degeneration when present in trans with a wild-type allele nor common polymorphisms. Two of the other 4 mutations have been reported previously as pathogenic (see mitodyn.org/home.php?select_db=OPA1 and figure 1C). For protein alignments, see figure e-1B.

and 3A,b, respectively). Increased colocalization of mitochondria with LC3/LysoID-positive autolysosomes supported an increase in mitophagy in these biallelic patients (figure 3A.c). Figure 3B shows that the increase in mean level of mitophagy in the group of all DOA plus patients (combining biallelic and monoallelic) compared to controls over 4 independent experiments was significantly increased ($p = 0.035$). It was not increased in nonsyndromic monoallelic relatives. Analysis of control fibroblasts treated with *OPA1* siRNA also suggested that mitophagy was increased compared with scramble siRNA (figure 3C.a). This is consistent with the increase in LC3-II abundance on Western blot analysis (figure 3C.b).

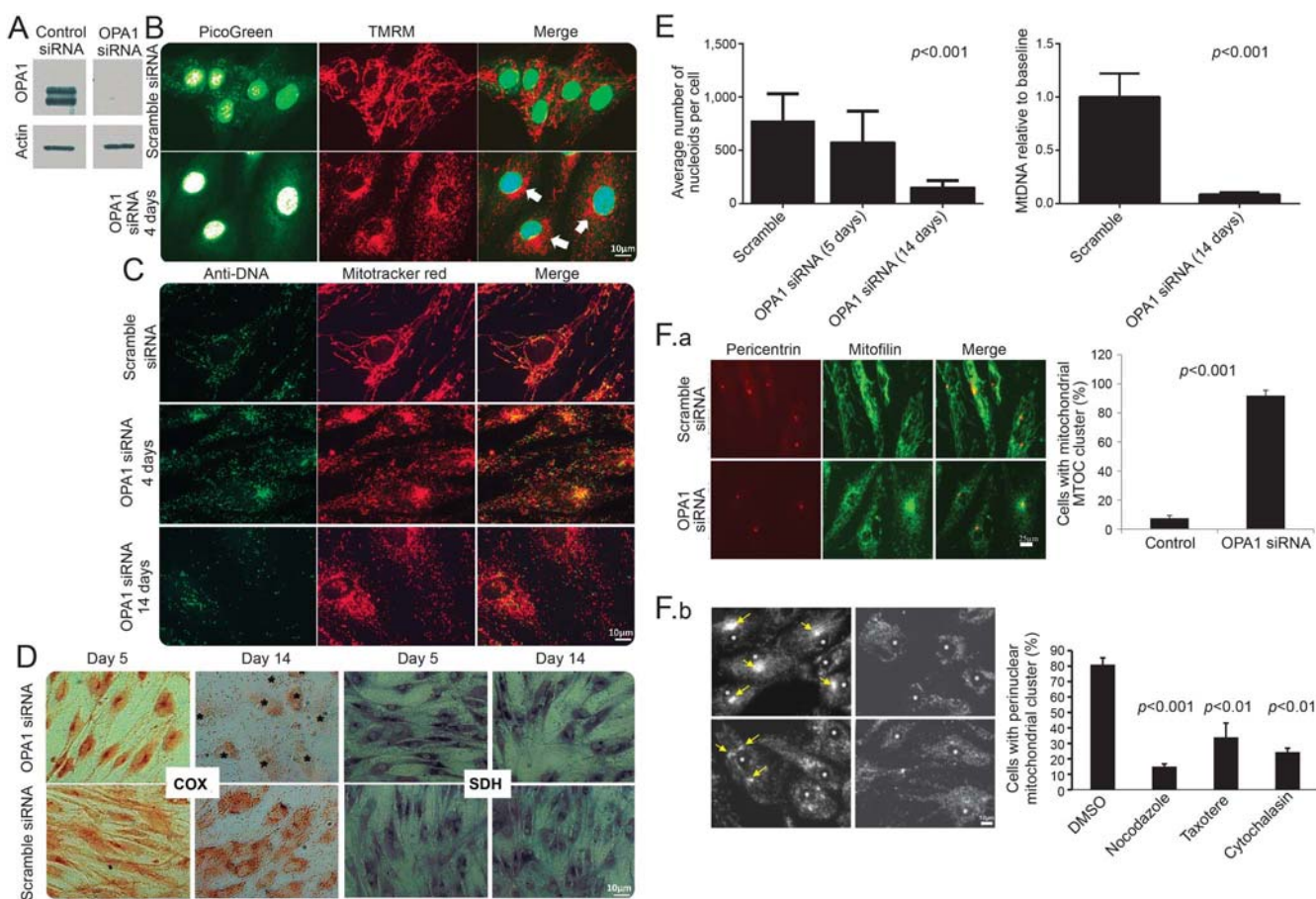
Similarly, quantitative fluorescence microscopy using IN Cell 1000¹⁶ confirmed that LC3 puncta colocalizing with mitochondria were increased in cells from biallelic patients at baseline, compared to controls (figure 3D). Similar increases in basal mitophagy were seen in fibroblasts from 2 monoallelic DOA plus *OPA1*(+/-) patients who had GTPase domain mutations (DOA plus *OPA1*[+/-]1 and DOA plus *OPA1*[+/-]2), but were comparable to control levels in cells from 5 individuals who had monoallelic *OPA1* mutations (N1, N2, *OPA1*[+/-]1, *OPA1*[+/-]2, and DOA *OPA1*[+/-]).

Mitophagic flux is increased in fibroblasts from biallelic DOA plus patients. An increase in autophagosomes could reflect either increased autophagic activity or a reduced turnover; we therefore measured mitophagic flux. This is defined as the ratio of the magnitude of the increase in counts of puncta colocalizing with mitochondria over basal levels, relative to basal mitophagy,² in a range of culture conditions and in the presence of lysosomal inhibitors. Growing fibroblasts on starvation (culture in minimal medium) or glucose-free galactose-based media (henceforth galactose medium) forces mitochondria to use oxidative phosphorylation and increases mitophagy.¹⁶ These culture conditions both generated a greater increase in colocalizing puncta in biallelic patients than in controls on both ImageStream (figure 3A) and IN Cell 1000 (figures 3D and 4B and not shown). Lysosomal inhibitors had a similar effect (figures 3, A, B, and D, and e-4).

Such conditions may also activate autophagy, consistent with the increase in LC3-II seen on Western analysis of cells cultured in galactose (figure e-5), but this increase is less reproducible.

Effect of *OPA1* mutations on mitophagy is modulated by knocking down proteins involved in mitophagy. To confirm that the increased colocalization of LC3 puncta

Figure 2 A reduction in OPA1 leads to rapid loss of mitochondrial DNA (mtDNA)



Control fibroblasts were treated with OPA1 Pan OPA1 or scramble siRNA. (A) Western blot analysis confirms OPA1 levels were efficiently reduced following siRNA treatment (blot shows 3 days after knockdown). (B) PicoGreen/tetramethyl rhodamine methyl ester (TMRM) costaining of live fibroblasts treated with OPA1 siRNA shows a marked loss of mtDNA nucleoids (visible as green puncta) compared to treatment with scramble. In all OPA1 knockdown cells with mitochondrial fragmentation, a noticeable mitochondrial perinuclear clustering was observed (arrows). (C) Anti-DNA/MitoTracker colabeling of OPA1/scramble siRNA treated fibroblasts (note that this antibody is recognized to label mtDNA more strongly than nuclear DNA). This confirms the findings presented in B. (D) Cytochrome oxidase (COX) activity, demonstrated by routine histochemistry, is significantly reduced by day 14. In the panel showing COX at 14 days in the knockdown, the positions of nuclei are marked with asterisks. By day 5, the distribution of both COX and succinate dehydrogenase (SDH) activity reflect the mitochondrial perinuclear clustering. Figure e-6 shows that mitochondrial fragmentation occurred without loss of cytochrome c or alteration of cristae at 48 hours. (E) SiRNA to OPA1 significantly reduced the number of nucleoids visualized by PicoGreen (left panel, $p < 0.001$, 2-tailed t test) corresponding to mtDNA content of $8\% \pm 2\%$ of the control. This was confirmed by quantitative PCR 14 days after treatment (right panel, $p < 0.001$, 2-tailed t test). (F) Cell biological basis for relocalization of mitochondria during OPA1 knockdown implies altered transport of fragmented mitochondria. OPA1 knockdown relocates mitochondria to the microtubule organizing center (MTOC), mediated by microtubules and actin. That this is prevented by overexpression of p50-dynamitin is shown in figure e-3B. (F.a) Anti-pericentrin (MTOC)/mitofillin (mitochondria) staining shows that siRNA to OPA1 causes relocation of mitochondria to the MTOC in over 90% of cells as opposed to the scrambled siRNA control (see chart). (F.b) The cell biological basis for relocalization of mitochondria during OPA1 knockdown implies altered transport mediated by microtubules and actin. Upper left: confirms the presence of perinuclear mitochondrial clusters following OPA1 knockdown. Upper right: Disassembly of microtubules by nocodazole treatment (5 μ M, 24 hours) rescues the mitochondrial clustering ($p < 0.001$). Lower left: Taxotere (5 μ M, 24 hours) causes assembly and stabilization of microtubules and hence randomly distributed mitochondrial clusters (3 clusters in one cell each marked with an arrow, $p < 0.01$). Lower right: Treatment with cytochalasin D (5 μ M, 24 hours), which depolymerizes actin, also redistributes mitochondria away from the MTOC, although a weak perinuclear clustering was still present ($p < 0.01$). Each of these experiments was carried out at least 3 times.

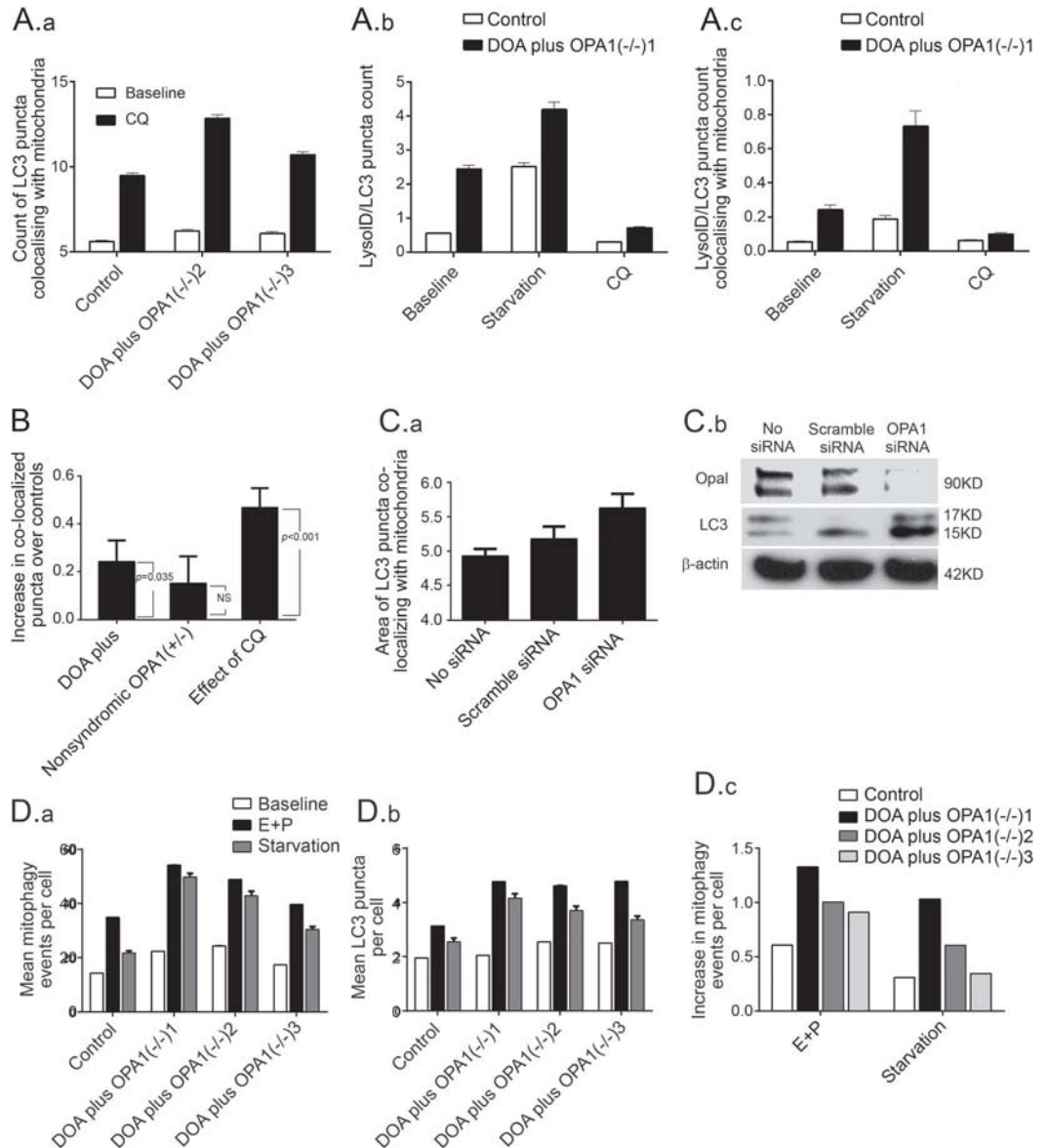
with mitochondria involved mitophagy, we knocked down the essential autophagy protein ATG7⁴ (figure 4A). We therefore performed RNAi on fibroblasts from DOA plus OPA1(-/-)1-3 patients and controls, obtaining a good reduction in ATG7 protein levels (figure 4A). Both total and colocalizing LC3 puncta were reduced by ATG7 knockdown in all conditions ($p < 0.001$, figure 4B), eliminating the difference between biallelic patients and controls,

both at baseline and after addition of the lysosomal inhibitors E64D and pepstatin A.

Effect of idebenone. Exposure of fibroblasts to idebenone, which modulates the increased mitophagy that we demonstrated in LHON,⁶ had no effect (figure e-4B).

A mitofusin 2 mutation increases mitochondrial fragmentation and mitophagy. Mitochondrial depolarization and ubiquitination are accepted triggers

Figure 3 Analysis of primary cultures from biallelic dominantly inherited optic atrophy (DOA) plus *OPA1*(-/-) patients demonstrates increased mitophagy compared to an age-matched control



(A) ImageStream analysis of cultured fibroblasts shows that basal mitophagy is significantly increased in DOA plus *OPA1*(-/-)2 and DOA plus *OPA1*(-/-)3 compared with control both at baseline and following treatment with CQ (all $p < 0.01$, 2-tailed t test). (A.a) The number of puncta per cell that were positive for light chain 3 (LC3) (representing both autophagosomes and autolysosomes) and Tom20 (representing mitochondria). These were counted at baseline in control cells, for comparison with patients DOA plus *OPA1*(-/-)2 and 3. Exposure to chloroquine (CQ; 25 μ M) overnight blocks mitophagy at this stage by preventing lysosomal acidification increasing the signal, more so in patients than controls. (A.b, A.c) The counts of puncta that are positive for both LC3 and LysolD (representing only autolysosomes), counted in control cells, for comparison with patient DOA plus *OPA1*(-/-)1. (A.b) The total number of puncta per cell that were positive for the autolysosome markers. (A.c) The counts of these autolysosomes that colocalized with mitochondria (hence autolysosomes involved in mitophagy) for the same dataset. In all cases there were more counts in the patient than the control. Galactose-based starvation medium increased the number of LC3/LysolD-positive puncta above baseline. Exposure to 25 μ M CQ overnight did not increase the signal, because it prevents progression of autophagosomes to autolysosomes. Error bars are standard errors (SEs) (technical replicates). Patient values all significantly greater than control $p < 0.01$ (2-tailed t test). All are representative of 1 out of 3 independent replicates. (B) A statistical analysis of 4 consecutive ImageStream runs on all the patients listed in the table along with 6 controls. The output shows increased mitophagy in patients with severe *OPA1* mutations (both biallelic and monoallelic, that is, DOA plus *OPA1*(-/-) and DOA plus *OPA1*(+/-)) compared with normal controls ($p = 0.035$). We show one bar per patient group, with each bar's height (y axis) representing the estimated difference between a particular patient group and controls. The whiskers on a bar represent the SE of the estimated difference (± 1 SE is shown); an approximate 95% confidence interval for the patient-control difference could be calculated as the bar height ± 2 SEs. The p values in the figure are from the test of the null hypothesis that there is no actual difference

Continued

for mitophagy, in some situations mitophagy being amplified by ubiquitinylation of the outer membrane proteins, mitofusin 1 and 2,²⁵ by Parkin, a ubiquitin ligase recruited to depolarized mitochondria in connection with PTEN-induced putative kinase 1 (PINK1).^{26,27}

Neither mitochondrial depolarization nor ubiquitination were apparent in our patient fibroblasts (figure 1E and not shown), so we questioned whether mitochondrial fragmentation was sufficient in itself to trigger mitophagy. We therefore studied fibroblasts from a patient with a dominant negative mutation in another mitochondrial pro-fusion gene, mitofusin 2 (*MFN2*). These fibroblasts showed increased fragmentation of mitochondria compared to controls ($p = 0.05$), associated with increased mitophagy, both at baseline and after treatment with the lysosomal inhibitor, chloroquine ($p < 0.02$ and 0.001 , respectively, figure 4C).

DISCUSSION We showed that profound loss of *OPA1* has several effects beyond mitochondrial fragmentation that potentially contribute to the pathogenesis of DOA and the onset of clinical disease. These include increased mitophagy, mitochondrial mislocalization, and, potentially, mitochondrial dysfunction due to mosaic mtDNA depletion.

We identified 3 patients who each carried one frameshift mutation in trans with a novel missense mutation, designated biallelic *OPA1*. The term Behr syndrome has been used for other biallelic *OPA1* families with severe phenotypes in which a missense allele, described as hypomorphic, occurs in trans with a pathogenic allele.²⁸ Furthermore, both frameshift mutations caused nonsyndromic DOA with incomplete penetrance, yet caused DOA plus when combined with a missense mutation.

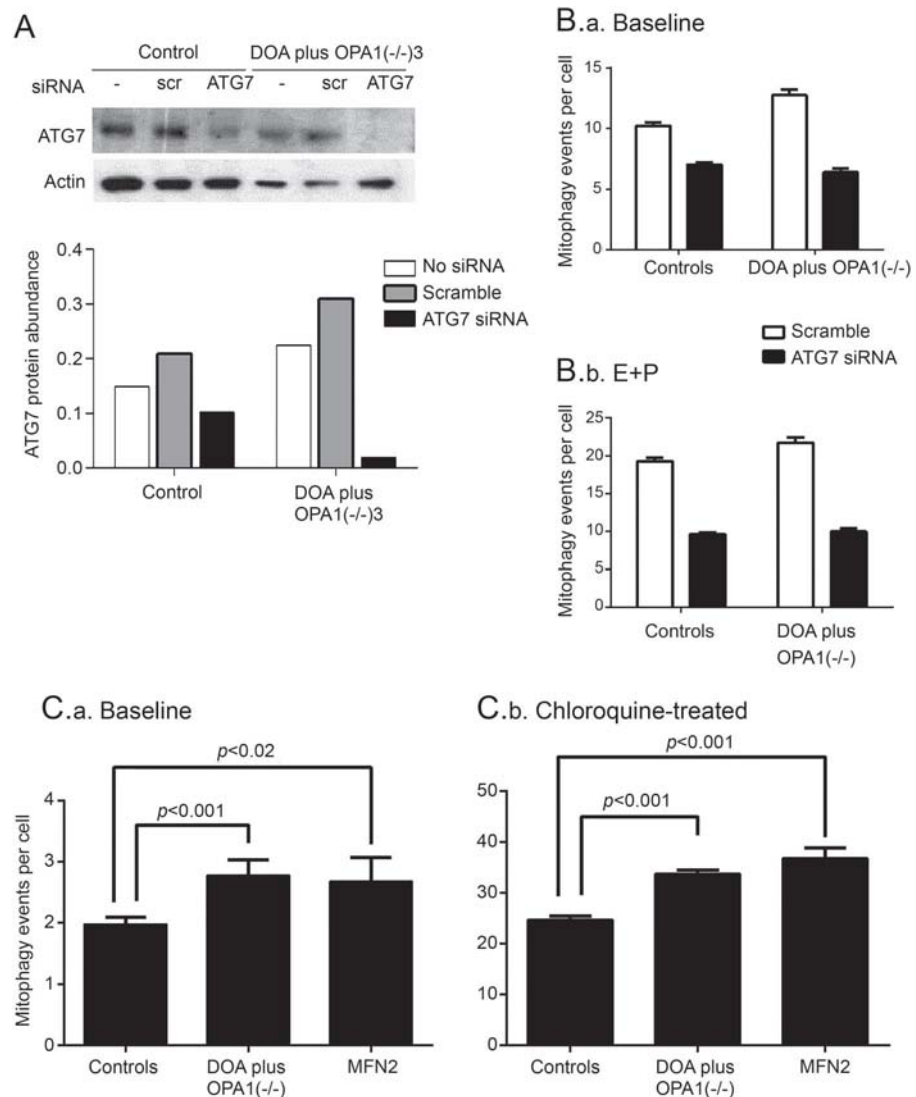
OPA1 is a transmembrane protein embedded within the inner mitochondrial membrane (IMM), involved in mitochondrial dynamics, specifically in IMM fusion²⁹ and maintenance of cristae. It is protective against apoptosis³⁰ and neurodegeneration.³¹ Mutant cells derived from patients with biallelic *OPA1* mutations not only had a lower level of *OPA1* protein, but there was evidence of significant mitochondrial fragmentation compared with controls (figure 1D). A small proportion of these cells with fragmented mitochondria were profoundly depleted of mtDNA (figure 1, C and E). High-throughput quantitative imaging revealed that mitochondrial fragmentation and mtDNA depletion was also increased in monoallelic DOA plus patients with dominantly inherited *OPA1* mutations involving the GTPase domain. While *OPA1* depletion is known to cause mtDNA depletion in neurons,³² the association in fibroblasts is novel. In line with other investigators, fragmentation and mtDNA depletion (figure 1E) were not present in fibroblast cultures from nonsyndromic DOA patients, from the asymptomatic, obligate carrier relatives of biallelic patients, or from the controls (table).

Previous investigators found that cultured cells with even severe respiratory chain defects appear to experience rather small increases in mitophagy³³ and that defects in respiratory chain function, if present in *OPA1* patients,¹⁴ are subtle.⁷ We suggest that these subtle defects may reflect the increased level of mtDNA-depleted mitochondria in cells that we documented. Two high-throughput imaging systems (ImageStream and IN Cell 1000) provide objective evidence of increased colocalization of mitochondria with autophagosomes and autolysosomes. These are more sensitive and specific for measuring mitophagy than conventional fluorescence and electron microscopy and Western blotting. Both methods showed

Figure 3 legend, continued:

between a patient group and controls. Useful intuition connecting the hypothesis test with the estimated difference is that a p value < 0.05 corresponds to a 95% confidence interval not overlapping zero. Uncomplicated symptomatic DOA *OPA1* (+/-) and asymptomatic *OPA1* (+/-) were not different from controls ($n = 1, 2,$ and $6,$ respectively). Chloroquine $25 \mu\text{M}$ overnight CQ significantly increased the number of LC3 puncta colocalizing with the mitochondrial signal in all individuals in all experiments ($p < 0.001$). (C) *OPA1* knockdown by siRNA also increases mitophagy. (C.a) Bar chart of ImageStream output shows that siRNA to *OPA1* increases mitophagy. The summed area of LC3 puncta that colocalize with mitochondria (PDH signal) in fibroblasts treated with *OPA1* siRNA is greater than in scramble siRNA and the untreated controls ($p = 0.05$ and $p < 0.01$, respectively, both 2-tailed t tests). Mitochondrial mean intensity was also reduced by 5% (not shown). Error bars are SEs (technical replicates). (C.b) In *OPA1* knockdown fibroblasts (*OPA1* siRNA) compared to untreated (No siRNA) and siRNA scramble (Scr siRNA) controls, *OPA1* levels are reduced and LC3-II levels are substantially increased relative to actin by the Western blot analysis. (D) Validation of the increased mitophagic flux, using IN Cell 1000 quantitative fluorescence microscopy. The number of LC3-positive puncta per cell was quantitated in fibroblasts from biallelic *OPA1* patients at baseline and after 2 hours in the presence of lysosomal protease inhibitors (E64D and pepstatin A, labeled E+P) or after 2 hours starvation in minimal medium compared with age-matched controls. (D.a) Per cell count of LC3-positive puncta colocalizing with mitochondria ($p < 0.0001$ and $p < 0.005$ for baseline compared to lysosomal inhibitors or starvation, respectively). (D.b) Mean number of total LC3-positive puncta per cell. Each patient had significantly higher counts than control ($p < 0.02$) in all conditions, except baseline patient DOA plus *OPA1*(-/-)3 autophagy and baseline patient DOA plus *OPA1*(-/-)1 mitophagy. (D.c) The mitophagic flux is increased in biallelic patients relative to controls (the increase in colocalization during starvation or lysosomal inhibitors, relative to baseline). Error bars are SEs of technical replicates, all p values 2-tailed t tests. For further evidence of increased mitophagic flux, see figure e-4A.

Figure 4 Effect of *OPA1* mutations on mitophagy is impaired by knockdown of *ATG7* and recapitulated by a mitofusin 2 (*MFN2*)-dominant negative genotype



(A) Western blot analysis confirms that knockdown of *ATG7* by siRNA reduced protein abundance relative to actin in both patient and control cells. *ATG7* = siRNA to *ATG7*; DOA = dominantly inherited optic atrophy; scr = scramble; siRNA = no treatment. (B) The number of colocalizing mitochondrial puncta (mitophagy events per cell, measured by IN Cell 1000) is significantly increased in fibroblasts from biallelic patients compared to controls at baseline (B.a) ($p < 0.001$) and after blocking autophagy with lysosomal inhibitors E64D and pepstatin A (E+P, $p = 0.01$). (B.b) Adding E64D and pepstatin A significantly increased the numbers of colocalizing puncta ($p < 0.001$) compared to baseline. Knockdown of *ATG7* protein by siRNA significantly reduced the colocalizing puncta ($p < 0.001$) and eliminated the increase in patients over controls. Cells were treated with siRNA against *ATG7* for 48 hours, then the medium was changed and either solvent or lysosomal inhibitors, E64D, and pepstatin A were added for 3 days. Error bars are standard errors of technical replicates, all p values 2-tailed t tests. (C) The number of mitophagy events per cell (measured by IN Cell 1000) at baseline (C.a) is significantly increased in fibroblasts from biallelic DOA plus *OPA1*(-/-) patients ($n = 3$) and in a patient with a dominant negative *MFN2* mutation compared to control ($p < 0.001$ and $p < 0.02$, respectively). After adding chloroquine (C.b), this was significantly increased in both the DOA plus *OPA1*(-/-) patients ($n = 3$) and the *MFN2* fibroblasts compared to control (both $p < 0.001$). In neither case was the *MFN2* significantly different from biallelic DOA plus *OPA1*(-/-) patients. Error bars are standard errors of technical replicates, all p values 2-tailed t tests.

that mitophagy is increased at baseline and following activation of autophagy in biallelic DOA plus fibroblasts, and is reduced by knockdown of the autophagy protein *ATG7* (figures 4, A and B, and e-2E). The increased colocalization of mitochondria and autophagosomes represents increased mitophagic flux

(figure e-4). Mitophagy was thus clearly increased in patients with monoallelic DOA plus and in severely affected biallelic *OPA1* patients, but not significantly in our monoallelic unaffected participants or in mildly affected, nonsyndromic monoallelic *OPA1* patients. The abundance of *OPA1* protein

reflected these differences (figure e-5). This is supported by electron microscopic findings in 2 mouse models.^{17,34}

Because mitophagy does not appear to increase bulk turnover of all mitochondrial components,³⁵ its importance has been called into question. It is the only type of mitochondrial quality control known to turn over whole mitochondrial genomes. While it is not clear that *OPA1* mutations directly cause mtDNA mutations or depletion, altering the dynamic cycle of mitochondrial fission and fusion is likely to dysregulate mitophagy and impair mitochondrial quality.³⁶

Our data show that active mitophagy closely reflects the phenotypic severity of DOA plus due to *OPA1* depletion (figures 1E, 3B, and e-5). We suggest 3 ways in which these could be linked (figure e-7).

First, the increased mitophagy may be driven by an excess of fragmented mitochondria, potentially because of a respiratory chain defect that we did not detect. This could be beneficial or neutral. This increase is consistent with type 1 mitophagy,³⁷ a subtype that is independent of *PINK1* and *Parkin*.³⁷ This is because we found no evidence of increased ubiquitination (not shown) and no recruitment of the mitophagy proteins *PINK1* and *Parkin*. It is thus plausible that increased fragmentation drives type 1 mitophagy.

Further, microtubule-dependent clustering of mitochondria, which is also apparent in *MFN2* knockdown,³⁸ may also disadvantage the cell, representing a mitophagic traffic jam. For instance, clustering of fragmented mitochondria may mechanically obstruct axonal transport of functioning mitochondria or prevent mitochondrial responses to stress (stress-induced mitochondrial hyperfusion³⁹).

Third, activated mitophagy may increase turnover of mitochondria and mtDNA. We showed that profound *OPA1* knockdown in control fibroblasts causes progressive loss of mtDNA and eventually mitochondrial function (figure 2E). Mitophagy may be excessive in retinal ganglion cells of *OPA1* patients, perhaps increasing demand on lysosomal pathways or causing mtDNA depletion in key locations. Indeed, *OPA1* depletion recapitulates the effects of the mitophagy-activating drug, phenanthroline. By disrupting *OPA1* processing, this metalloprotease inhibitor activates mitophagy excessively, depleting mitochondria and mtDNA and impairing the selectivity for damaged mtDNA.¹⁶

The interplay between these mechanisms remains to be determined (figure e-7). We showed evidence that *OPA1* depletion affects mitochondrial fragmentation, quality control, and likely microtubular transport, all important determinants of mitochondrial

mass,⁴⁰ neuronal maturation,³² and health.³ These could underline the known effects of *OPA1* depletion on neural maturation,³² leading to retinal ganglion cell loss, optic nerve degeneration, and hence visual failure. In particular, increased mitophagy is implicated in both LHON and syndromic parkinsonism caused by *OPA* mutations.⁸ These add biological credibility to our suggestion that dysregulated mitophagy is important in the pathogenesis of mitochondrial optic neuropathies.⁶ If so, drug modulators of mitophagy may be useful therapies for this group of disorders.

AUTHOR AFFILIATIONS

From the Nuffield Department of Obstetrics and Gynaecology (C. Liao, N.A., A.D., K.M., L.V., J.C., E.D., J.P.), The Women's Centre; Nuffield Department of Medicine (K.P., A.K.S.), NIHR Translational Immunology Laboratory Biomedical Research Centre, Oxford; Departments of Paediatrics and Ophthalmology and Virtual Academic Unit (A.W., I.F.), Northampton General Hospital; Institute of Medical Genetics (L.R.) and Cardiff Eye Unit (M.V.), University Hospital of Wales, Cardiff; Department of Clinical Genetics (J.L.) and Oxford Medical Genetics Laboratories (C.F.), Churchill Hospital; Nuffield Division of Clinical Laboratory Sciences (D.J.P.F.); Department of Neuroradiology (G.Q.), Oxford University Hospitals NHS Trust, UK; Department of Child Neurology (I.M.) and Division of Molecular Neurogenetics (C. Lamperti), Carlo Besta Neurological Institute IRCCS; Service of Neuro-ophthalmology and Eye Electrophysiology (S.B.), The Auxologico Institute IRCCS, Milan, Italy; Department of Ophthalmology (S.M.D.), John Radcliffe Hospital, Oxford; Wellcome Trust Centre for Mitochondrial Research (K.S.S., P.J.F., P.Y.-W.-M.), Institute of Genetic Medicine, Newcastle University, Newcastle upon Tyne; Department of Comparative Biomedical Sciences (D.E., M.C.), The Royal Veterinary College, University of London; MRC Centre for Neuromuscular Disorders (M.L., M.M.R.), Department of Molecular Neurosciences, UCL Institute of Neurology, Queen Square, London; Sheffield Institute for Translational Neuroscience (H.M.), University of Sheffield; CRUK/MRC Oxford Institute for Radiation Oncology (R.P.) and Division of Cardiovascular Medicine, Radcliffe Department of Medicine (M.J.D.), University of Oxford; UCL Consortium for Mitochondrial Research (M.C.), London; MRC Mitochondrial Biology Unit (M.Z.), Cambridge; Newcastle Eye Centre (P.Y.-W.-M.), Royal Victoria Infirmary, Newcastle upon Tyne, and NIHR Biomedical Research Centre at Moorfields Eye Hospital and UCL Institute of Ophthalmology, London; and School of Optometry and Vision Sciences (M.V.), Cardiff University, UK. L.V. is currently affiliated with the Molecular, Cellular and Developmental Neurobiology Department, Cajal Institute-CSIC, Madrid, Spain.

AUTHOR CONTRIBUTIONS

Chunyan Liao: acquisition and analysis of data. Neil Ashley: acquisition and analysis of data. Alan Diot: acquisition and analysis of data. Karl Morten: acquisition and analysis of data. Kanchan Phadwal: acquisition and analysis of data. Andrew Williams: clinical description of patient. Ian Fearnley: clinical description of patient. Lyndon Rosser: acquisition and analysis of data. Jo Lowndes: clinical description of patient. Carl Fratter: acquisition and analysis of data. David Ferguson: acquisition and analysis of data. Laura Vay: acquisition and analysis of data. Gerardine Quaghebeur: clinical description of patient. Isabella Moroni: clinical description of patient. Stefania Bianchi: clinical description of patient. Costanza Lamperti: clinical description of patient. Susan Downes: clinical description of patient. Kamil S. Sitarz: acquisition and analysis of data. Pdraig J. Flannery: acquisition and analysis of data. Janet Carver: acquisition and analysis of data. Eszter Dombi: acquisition and analysis of data. Daniel East: acquisition and analysis of data. Matilde Laura: characterization of patient cells. Mary M. Reilly: characterization of patient cells. Heather Mortiboys: acquisition and analysis of data. Remko Prevo: acquisition and analysis of data.

data. Michelangelo Campanella: acquisition and analysis of data. Matthew Daniels: acquisition and analysis of data. Massimo Zeviani: critical revision of the manuscript. Patrick Yu-Wai-Man: clinical description of patient and critical revision of the manuscript. Anna Katharina Simon: critical revision of the manuscript. Marcela Votruba: critical revision of the manuscript. Joanna Poulton: supervisor role, critical revision of the manuscript, design and conceptualization of the study.

ACKNOWLEDGMENT

The authors thank the patients and their families for participating, Daniele Ghezzi for help with bioinformatics, Aviva Tolkovsky for expert advice, Rebecca Muir and Pippa Oakeshott for proofing, and Stephen Kennedy for support.

STUDY FUNDING

This work was supported by the Oxford Partnership Comprehensive Biomedical Research Centre with funding from the Department of Health's NIHR Biomedical Research Centres funding scheme, NewLife, the MRC (MR/J010448/1), the Wellcome Trust (0948685/Z/10/Z) and the Angus Memorial Mitochondrial Fund. J.P., J.L., J.C., and C.F. have salary support from the NHS Specialized Services Rare Mitochondrial Disorders Service. K.P. and A.K.S. were funded by the NIHR Biomedical Research Center Oxford. P.Y.-W.-M. is supported by a Clinician Scientist Fellowship Award (G1002570) from the Medical Research Council (MRC, UK) and receives funding from Fight for Sight (UK), the UK National Institute of Health Research (NIHR) as part of the Rare Diseases Translational Research Collaboration, and the NIHR Biomedical Research Centre based at Moorfields Eye Hospital NHS Foundation Trust and UCL Institute of Ophthalmology. The views expressed are those of the authors and not necessarily those of the NHS, the NIHR, or the Department of Health.

DISCLOSURE

C. Liao was funded by the Wellcome Trust (0948685/Z/10/Z). N. Ashley reports no disclosures relevant to the manuscript. A. Diot was funded by the MRC (MR/J010448/1) and the NewLife Foundation. K. Morten was funded by the Williams Foundation. K. Phadwal was funded by the NIHR Biomedical Research Centre, Oxford. A. Williams, I. Fearnley, L. Rosser, J. Lowndes, C. Fratter, D. Ferguson, L. Vay, G. Quaghebeur, I. Moroni, S. Bianchi, C. Lamperti, S. Downes, K. Sitarz, and P. Flannery report no disclosures relevant to the manuscript. J. Carver was funded by the MRC (MR/J010448/1). E. Dombi was funded by the Lily Foundation, the Angus Memorial Mitochondrial Fund, and the NewLife Foundation. D. East, M. Laura, M. Reilly, H. Mortiboy, R. Prevo, and M. Campanella report no disclosures relevant to the manuscript. M. Daniels reports sponsorship from the Wellcome Trust (WT098519MA). M. Zeviani reports no disclosures relevant to the manuscript. P. Yu-Wai-Man holds a consultancy agreement with GenSight Biologics (Paris, France). A. Katharina Simon was funded by the NIHR Biomedical Research Centre, Oxford. M. Votruba reports no disclosures relevant to the manuscript. J. Poulton was funded by the Wellcome Trust (0948685/Z/10/Z), the MRC (MR/J010448/1), Lily Foundation, the Angus Memorial Mitochondrial Fund, and the NewLife Foundation. Go to Neurology.org for full disclosures.

Received July 5, 2016. Accepted in final form October 4, 2016.

REFERENCES

- Gomes LC, Di Benedetto G, Scorrano L. During autophagy, mitochondria elongate are spared from degradation and sustain cell viability. *Nat Cell Biol* 2011;13:589–598.
- Klionsky DJ, Abdelmohsen K, Abe A, et al. Guidelines for the use and interpretation of assays for monitoring autophagy (3rd edition). *Autophagy* 2016;12:1–222.
- Rugarli EI, Langer T. Mitochondrial quality control: a matter of life and death for neurons. *EMBO J* 2012;31:1336–1349.

- Mortensen M, Ferguson DJ, Edelmann M, et al. Loss of autophagy in erythroid cells leads to defective removal of mitochondria and severe anemia in vivo. *Proc Natl Acad Sci USA* 2010;107:832–837.
- Dai Y, Zheng K, Clark J, et al. Rapamycin drives selection against a pathogenic heteroplasmic mitochondrial DNA mutation. *Hum Mol Genet* 2014;23:637–647.
- Dombi E, Diot A, Morten K, et al. The m.13051G>A mitochondrial DNA mutation results in variable neurology and activated mitophagy. *Neurology* 2016;86:1921–1923.
- Amati-Bonneau P, Guichet A, Olichon A, et al. *OPA1* R445H mutation in optic atrophy associated with sensorineural deafness. *Ann Neurol* 2005;58:958–963.
- Carelli V, Musumeci O, Caporali L, et al. Syndromic parkinsonism and dementia associated with *OPA1* missense mutations. *Ann Neurol* 2015;78:21–38.
- Longatti A, Orsi A, Tooze SA. Autophagosome formation: not necessarily an inside job. *Cell Res* 2010;20:1181–1184.
- Korolchuk VI, Saiki S, Lichtenberg M, et al. Lysosomal positioning coordinates cellular nutrient responses. *Nat Cell Biol* 2011;13:453–460.
- Pesch UE, Leo-Kottler B, Mayer S, et al. *OPA1* mutations in patients with autosomal dominant optic atrophy and evidence for semi-dominant inheritance. *Hum Mol Genet* 2001;10:1359–1368.
- Schaaf CP, Blazo M, Lewis RA, et al. Early-onset severe neuromuscular phenotype associated with compound heterozygosity for *OPA1* mutations. *Mol Genet Metab* 2011;103:383–387.
- Yu-Wai-Man P, Griffiths PG, Gorman GS, et al. Multi-system neurological disease is common in patients with *OPA1* mutations. *Brain* 2010;133:771–786.
- Amati-Bonneau P, Valentino ML, Reynier P, et al. *OPA1* mutations induce mitochondrial DNA instability and optic atrophy “plus” phenotypes. *Brain* 2008;131:338–351.
- Yu-Wai-Man P, Sitarz KS, Samuels DC, et al. *OPA1* mutations cause cytochrome c oxidase deficiency due to loss of wild-type mtDNA molecules. *Hum Mol Genet* 2010;19:3043–3052.
- Diot A, Hinks-Roberts A, Lodge T, et al. A novel quantitative assay of mitophagy: combining high content analysis fluorescence with mitochondrial DNA mutant load to identify novel pharmacological modulators of mitophagy. *Pharmacol Res* 2015;100:24–35.
- Sarzi E, Angebault C, Seveno M, et al. The human *OPA1delTTAG* mutation induces premature age-related systemic neurodegeneration in mouse. *Brain* 2012;135:3599–3613.
- Ashley N, Harris D, Poulton J. Detection of mitochondrial DNA depletion in living human cells using PicoGreen staining. *Exp Cell Res* 2005;303:432–446.
- Uusimaa J, Evans J, Smith C, et al. Clinical, biochemical, cellular and molecular characterization of mitochondrial DNA depletion syndrome due to novel mutations in the *MPV17* gene. *Eur J Hum Genet* 2014;22:184–191.
- Elachouri G, Vidoni S, Zanna C, et al. *OPA1* links human mitochondrial genome maintenance to mtDNA replication and distribution. *Genome Res* 2011;21:12–20.
- Ashley N, Poulton J. Anticancer DNA intercalators cause p53-dependent mitochondrial DNA nucleoid re-modeling. *Oncogene* 2009;28:3880–3891.

22. Kimura S, Noda T, Yoshimori T. Dynein-dependent movement of autophagosomes mediates efficient encounters with lysosomes. *Cell Struct Funct* 2008;33:109–122.
23. Korolchuk VI, Rubinsztein DC. Regulation of autophagy by lysosomal positioning. *Autophagy* 2011;7:927–928.
24. Ebneth A, Godemann R, Stamer K, Illenberger S, Trinczek B, Mandelkow E. Overexpression of tau protein inhibits kinesin-dependent trafficking of vesicles, mitochondria, and endoplasmic reticulum: implications for Alzheimer's disease. *J Cell Biol* 1998;143:777–794.
25. Gegg ME, Cooper JM, Chau KY, Rojo M, Schapira AH, Taanman JW. Mitofusin 1 and mitofusin 2 are ubiquitinated in a PINK1/parkin-dependent manner upon induction of mitophagy. *Hum Mol Genet* 2010;19:4861–4870.
26. Narendra DP, Jin SM, Tanaka A, et al. PINK1 is selectively stabilized on impaired mitochondria to activate Parkin. *PLoS Biol* 2010;8:e1000298.
27. Narendra D, Tanaka A, Suen DF, Youle RJ. Parkin is recruited selectively to impaired mitochondria and promotes their autophagy. *J Cell Biol* 2008;183:795–803.
28. Carelli V, Sabatelli M, Carozzo R, et al. "Behr syndrome" with *OPA1* compound heterozygote mutations. *Brain* 2015;138:e321.
29. Mishra P, Carelli V, Manfredi G, Chan DC. Proteolytic cleavage of Opa1 stimulates mitochondrial inner membrane fusion and couples fusion to oxidative phosphorylation. *Cell Metab* 2014;19:630–641.
30. Olichon A, Landes T, Arnaune-Pelloquin L, et al. Effects of *OPA1* mutations on mitochondrial morphology and apoptosis: relevance to ADOA pathogenesis. *J Cell Physiol* 2007;211:423–430.
31. Civiletto G, Varanita T, Cerutti R, et al. Opa1 overexpression ameliorates the phenotype of two mitochondrial disease mouse models. *Cell Metab* 2015;21:845–854.
32. Bertholet AM, Millet AM, Guillermin O, et al. OPA1 loss of function affects in vitro neuronal maturation. *Brain* 2013;136:1518–1533.
33. Gilkerson RW, De Vries RL, Lebot P, et al. Mitochondrial autophagy in cells with mtDNA mutations results from synergistic loss of transmembrane potential and mTORC1 inhibition. *Hum Mol Genet* 2012;21:978–990.
34. White KE, Davies V, Hogan V, et al. OPA1 deficiency is associated with increased autophagy in retinal ganglion cells in a murine model of dominant optic atrophy. *Invest Ophthalmol Vis Sci* 2009;50:2567–2571.
35. Kim TY, Wang D, Kim AK, et al. Metabolic labeling reveals proteome dynamics of mouse mitochondria. *Mol Cell Proteomics* 2012;11:1586–1594.
36. Twig G, Elorza A, Molina AJ, et al. Fission and selective fusion govern mitochondrial segregation and elimination by autophagy. *EMBO J* 2008;27:433–446.
37. Lemasters JJ. Variants of mitochondrial autophagy: types 1 and 2 mitophagy and micromitophagy (type 3). *Redox Biol* 2014;2:749–754.
38. Baloh RH, Schmidt RE, Pestronk A, Milbrandt J. Altered axonal mitochondrial transport in the pathogenesis of Charcot-Marie-Tooth disease from mitofusin 2 mutations. *J Neurosci* 2007;27:422–430.
39. Tondera D, Grandemange S, Jourdain A, et al. SLP-2 is required for stress-induced mitochondrial hyperfusion. *EMBO J* 2009;28:1589–1600.
40. Giordano C, Iommarini L, Giordano L, et al. Efficient mitochondrial biogenesis drives incomplete penetrance in Leber's hereditary optic neuropathy. *Brain* 2014;137:335–353.

Neurology®

Dysregulated mitophagy and mitochondrial organization in optic atrophy due to *OPA1* mutations

Chunyan Liao, Neil Ashley, Alan Diot, et al.
Neurology published online December 14, 2016
DOI 10.1212/WNL.0000000000003491

This information is current as of December 14, 2016

Updated Information & Services	including high resolution figures, can be found at: http://www.neurology.org/content/early/2016/12/14/WNL.0000000000003491.full.html
Supplementary Material	Supplementary material can be found at: http://www.neurology.org/content/suppl/2016/12/14/WNL.0000000000003491.DC1.html
Subspecialty Collections	This article, along with others on similar topics, appears in the following collection(s): Mitochondrial disorders http://www.neurology.org/cgi/collection/mitochondrial_disorders Mitochondrial disorders; see Genetics/Mitochondrial disorders http://www.neurology.org/cgi/collection/mitochondrial_disorders_see_genetics-mitochondrial_disorders
Permissions & Licensing	Information about reproducing this article in parts (figures, tables) or in its entirety can be found online at: http://www.neurology.org/misc/about.xhtml#permissions
Reprints	Information about ordering reprints can be found online: http://www.neurology.org/misc/addir.xhtml#reprintsus

Neurology® is the official journal of the American Academy of Neurology. Published continuously since 1951, it is now a weekly with 48 issues per year. Copyright © 2016 The Author(s). Published by Wolters Kluwer Health, Inc. on behalf of the American Academy of Neurology. All rights reserved. Print ISSN: 0028-3878. Online ISSN: 1526-632X.



Supplementary information

Appendix e-1: Supplementary clinical and molecular information (see table 1)

Family 1 Clinical presentation

DOAplus OPA1(-/-)1 is a 17 year old Caucasian male from the UK, who presented with a severe phenotype due to OPA1 at the age of 10. As well as clumsiness and progressive unsteadiness, his mother reported worsening school performance and painful parasthesiae in his limbs. He admitted to loss of sensation in his hands and feet. He had developed poor vision in infancy, presenting aged 10 months with a convergent squint and corrective surgery aged 14 months. At aged 2 he was bumping into things, with progressive stepwise visual loss over 8 months. There was no relevant family history (Figure 1A).

On examination, he was a well grown boy without dysmorphic features. He had bilateral optic atrophy, but no ptosis and full eye movements. Visual acuities were finger counting in the left eye and less than this in the right. Flash electroretinograms indicated normal photoreceptor/outer retinal function, and visual evoked potentials were consistent with abnormal optic nerve conduction. Muscle bulk and power were normal, but with distal laxity in the upper limbs. In the lower limbs, he had slightly decreased ankle dorsiflexion and his reflexes were brisk with ankle clonus. He also had reduced sensation in all modalities tested, suggesting a sensory neuropathy. He was unsteady on his feet, but had no evidence of cerebellar ataxia. Cranial MRI (see below) showed very small optic nerves and chiasma. Electrophysiology showed an axonal neuropathy affecting sensory fibres more than motor. He subsequently continued to regress, developed epilepsy, and at 17 years is unable to walk independently. Neuropathic pain is now a major management problem and very recently he has developed gastrointestinal problems which are reported separately (1).

Both history and clinical examination of the proband's mother (N1, carrying c.661G>A p.E221K) and grandfather (OPA1(+/-)1 carrying c.2708_2711delTTAG OPA) were unremarkable, though the latter did not attend specialist ophthalmology appointments. The latter mutation has a known penetrance of approximately 55% (2).

Mitochondrial investigations, including blood and CSF lactate, muscle biopsy COX histochemistry and respiratory chain function, were normal. Mitochondrial DNA mutations were excluded, including screening skeletal muscle for mtDNA rearrangements by LPCR and full mtDNA sequencing. MtDNA copy number in skeletal muscle was 115% of expected and in fibroblasts 94%. In addition, nuclear DNA sequencing excluded mutations in the whole of the *POLG* and the mutation hotspot of the *PEO1* (TWINKLE) genes. The absence of mtDNA abnormalities seen in CPEO patients is probably because of his youth, and the normal respiratory chain results do not conflict with the subtle defects identified by others (33-37) (3).

Family 2 Clinical presentation

The proband, DOAplus OPA1(-/-)2, is a girl, now 12 years old, with a severe and progressive visual defect, born to non consanguineous Italian parents. Family history was negative for neurological and ophthalmologic diseases. Pregnancy and delivery were uneventful; psychomotor development was reported to be normal. Parents suspected poor vision from 3 years of age; the first ophthalmologic examination, at 6 years of age, confirmed a severe loss of visual acuity. Brain MRI was normal; visual evoked potentials revealed markedly reduced amplitudes; ERG was unremarkable. When first observed by us, at 8 years of age, the ophthalmologic evaluation revealed a marked pallor of the optic disc. Neurological examination showed bilateral *pes cavus* and reduced tendon reflexes in lower limbs, but no motor symptoms. EMG showed a reduction of Sensory Action Potentials in her lower limbs (6.0 μ V in peroneal nerves) with normal Sensory Conduction Velocities.

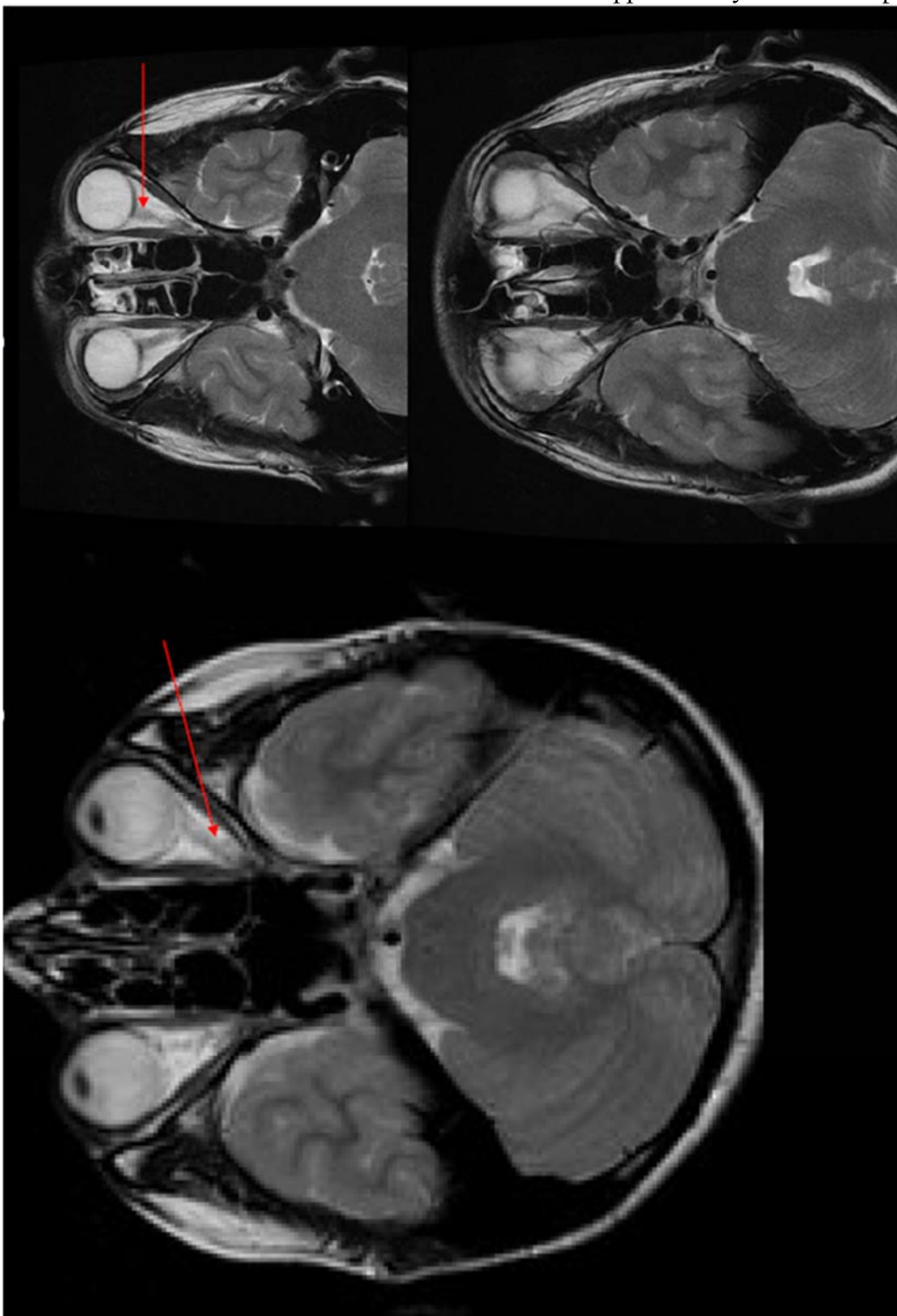
The brother, OPA1(-/-)3, now aged 6 years and 10 months, had an identical course to his sister. He was noted to have difficulties in watching the television since the second year of life. He was examined at 4 years of age and showed the presence of similar ophthalmologic signs (reduced visual acuity, and pale optic discs at fundus exam), without signs of neurological impairment. At the last observation at 6.5 years of age he also showed bilateral *pes cavus* with mild reduction of distal tendon reflexes in his lower limbs. Plasma lactate and pyruvate were both normal in both siblings.

The neurological and ophthalmological examination of both parents was normal at first consultation (father is designated N2 and the mother OPA1(+/-)2). At the last examination, the mother (aged 41) showed mild signs of optic atrophy, and a pathologically thin retinal

nerve fibre layer by optical coherence tomography retinal imaging. The father (aged 47) remains entirely normal. Recently a maternal aunt reported a visual defect.

Figure e-1A: MRI scan of patient DOAplus OPA1(-/-)1

MRI scan showed bilateral degeneration of the optic nerves (red arrows) which are very small. Proband on left, age matched “control” on right.



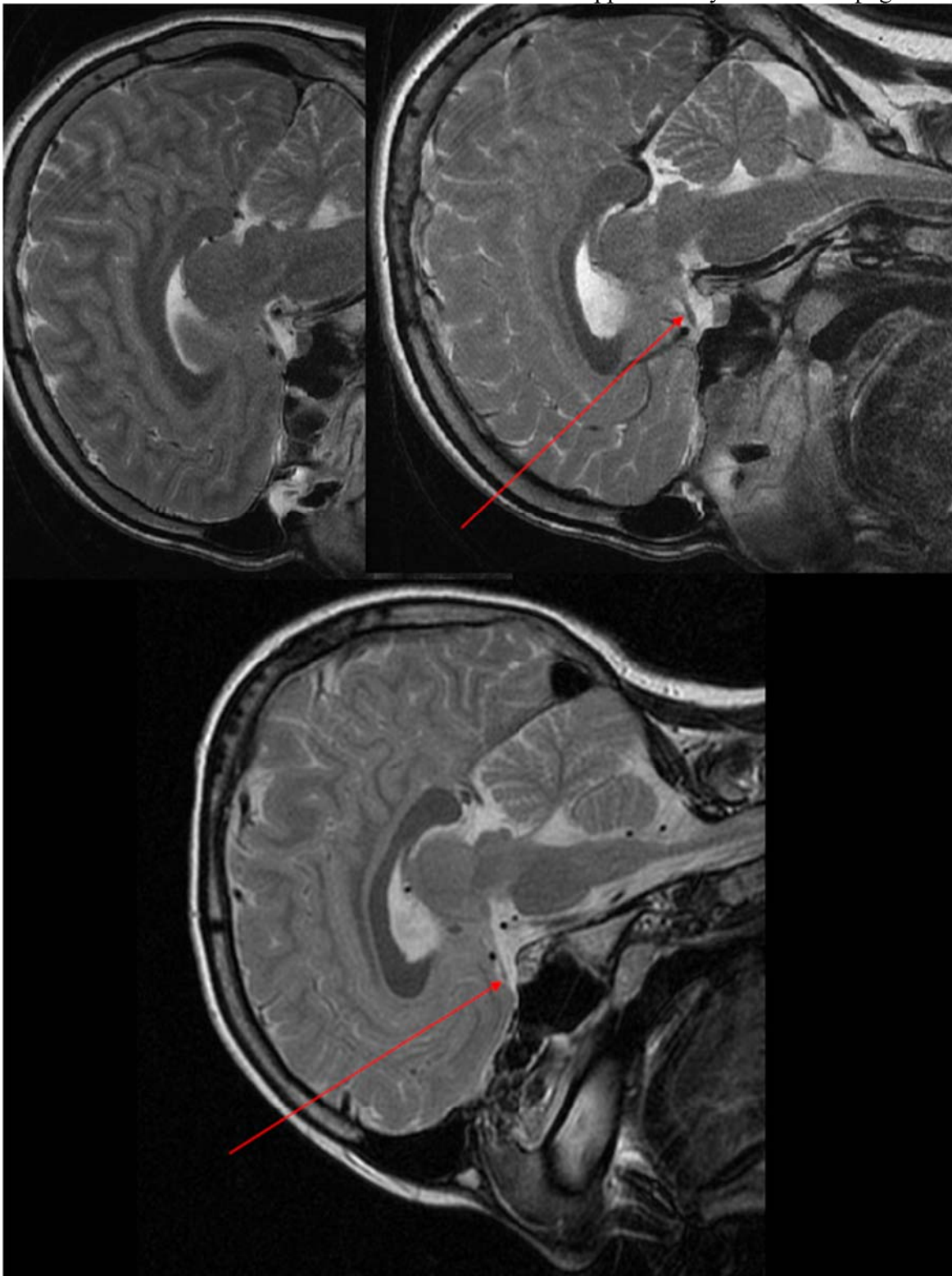


Figure e-1B

Further information about OPA1 variants identified in patients whose cell cultures were analysed in detail including protein alignments.

OPA1 sequence was used for the organisms listed, except for *D.Melanogaster*, *A.Gambiae* and *C.Elegans* where Opa1-like, AgaP_AGAP011286 and EAT-3 were used respectively. In *D.Rerio*, Opa1-like was used in addition to OPA1. In the bottom panel, the substituted residues are highlighted in yellow.

Family	Variant	Protein	Exon	SIFT prediction	Grantham difference	Species Conservation	Comments
1	c.2708_2711delTTAG	p.V903Gfs*3	27		N/A	N/A	Previously reported as pathogenic
1	c.661G>A	p.E221K	6	Predicted to affect protein function	56	Conserved across all species listed	Coiled-coil domain See alignment below left
2	c.2353delC	p.Q785Sfs*15	23		N/A	N/A	
2	c.2869C>T	p.H957Y	28	Predicted to affect protein function	83	Conserved in vertebrates (N in Fruitfly, Q in C. elegans, missing in yeast)	GTPase effector domain See alignment below right
3	c.876_878delTGT	p.V294del	9		N/A	Run of 4 valines is conserved to C. elegans	GTPase domain
4	c.1334G>A	p.R445H	14		29	Conserved to C. elegans	GTPase domain Previously reported as pathogenic

**c.661G>A
E221K**

H.sapiens	210	VSDKEKIDQLQEELLHTQLKYQRILERLEKENKELRK--LVLQKDDKGIH	257
F.troglodytes	210	VSDKEKIDQLQEELLHTQLKYQRILERLEKENKELRK--LVLQKDDKGIH	257
M.mulatta	246	VSDKEKIDQLQEELLHTQLKYQRILERLEKENKELRK--LVLQKDDKGIH	293
C.lupus	264	VIDKEKIDQLQEELLHTQLKYQRILERLEKENKELRK--LVLQKDDKGIH	311
B.taurus	246	VSDKEKIDQLQEELLHTQLKYQRILERLEKENKELRK--LVLQKDDKGIH	293
M.musculus	227	VSDKEKIDQLQEELLHTQLKYQRILERLEKENKELRK--LVLQKDDKGIH	274
R.norvegicus	209	VSDKEKIDQLQEELLHTQLKYQRILERLEKENKELRK--LVLQKDDKGIH	256
G.gallus	226	VSDKEKIDQLQEELLRQLKYQRMLE RLEKENKELRK--LVLQRDDKGIH	273
D.rerio	215	SSDKEKVDQLQEELLRQLKYQRMLE RLEKENKELRK--VVLQKDDKGIH	262
D.rerio	283	SSDKEKVDQLQEELLRQLKYQRMLE RLEKENKELRK--VVLQKDDKGIH	330
D.melanogaster	220	-KLSQVETLQTEIMNVQIKYQKELE RMEKENREL RQQYL I LKTNKKT-T	267
A.gambia	127	-TLQAQVDSLQTEIMNVQIKYQREVE KLEKENRDL RQQYL I LKTNRKQPT	175
C.elegans	207	VSAERIQKQLQEEMLKTQSQYQRELE RLEKENKVLKQR-LLSDDKKAIR	255

**c.2869C>T
H957Y**

953	FIEALHQEK-	961
953	FIEALHQEK-	961
989	FIEALHQEK-	997
1007	FIEALHQEK-	1015
989	FIEALHQEK-	997
970	FIEALHQEK-	978
952	FIEALHQEK-	960
969	FIEALHQEK-	977
958	FIEALHKEK-	966
1026	FIEALHKEK-	1034
964	FINSLNQEK-	972
871	FINALNLEK-	879
955	FMAQLQREKI	964

Figure e-2. Validation of ImageStream and further validation of INCell 1000 for detecting mitophagy

Figure e-2A Confocal imaging of mitophagy

Mouse embryonic fibroblasts expressing both dsred targeted to mitochondria and LC3 tagged with GFP were grown in regular medium (glucose) or in the presence of lysosomal inhibitors E64d and pepstatin A (Glucose E&P). After fixation, mitochondrial (dsred) and autophagosomes (GFP) signals were acquired on a Leica SP5 confocal microscope using a 63X lens and further digital zoom when needed. Arrowheads indicate autophagosomes engulfing mitochondria ie mitophagy (Glucose E&P zoomed in bottom panels).

Figure e-2B Mitophagy events per cell corresponding to the confocal images in part A were quantitated using IN Cell 1000.

This additional validation of IN Cell 1000 shows a significant increase in co-localisation of LC3 puncta with mitochondria in the presence of E64d and pepstatin A (E+P).

Figure e-2C Raw ImageStream output displaying 4 views on one gated cell. Channel 05 (Left) shows fibroblasts in bright field, channel 03 detects mitochondrial signal (PDH, Mitoscience) and channel 06 detects LC3 (Cell Signalling Technology), using anti-mouse Alexa-488 and anti-rabbit Alexa -546 secondary antibodies respectively (both Invitrogen). Ch03/Ch06 shows co-localisation of bright signal.

Figure e-2D: Using IN Cell 1000 to validate ImageStream

Cells that have been well characterised by confocal microscopy (4) were used to Validate ImageStream (right chart) against IN Cell 1000 (left chart). These cells are HeLa cells expressing dsred targeted to mitochondria and GFP-tagged either autophagosome marker LC3 or lysosomal marker CD63 (courtesy of Prof A Tolkovsky (4)). Figures 9 and 10 of that paper (4) follow mitophagy in real time by co-localisation of the mitochondrial dsred with these markers. Counts of GFP puncta (either LC3-labelled autophagosomes shown on the left of each plot, or autolysosome labelled with CD63 shown on the right of each plot) that are co-localised with mitochondria, thus reflect sequential stages of mitophagy. In corresponding ImageStream (C) and IN Cell 1000 experiments (D), the bar chart shows co-localisation of GFP puncta with mitochondrial (dsred) signal at baseline, in

the presence of either 3 days glucose-free galactose media (Gal) or following 16 hours exposure to chloroquine 25 μ M (Glu CQ). Chloroquine substantially increases the number of autophagosomes but not autolysosomes, galactose causes a more modest increase. The results in (C) and (D) look very similar, suggesting that both techniques are able to measure co-localisation of mitochondria with GFP puncta.

Error bars are standard errors of technical replicates.

Figure e-2E Knock out of the essential mitophagy protein, Atg7, in mouse splenocytes reduces co-localisation of LC3 and LysoID positive puncta with mitochondria, further validating the ability of ImageStream to detect mitophagy.

To validate that ImageStream is able to detect mitophagy we investigated mouse splenocytes, obtained from either wild type mice or from mice whose key autophagy gene, Atg7, has been excised in the haematopoietic system only (Vav-Atg7^{-/-}) (5) (6).

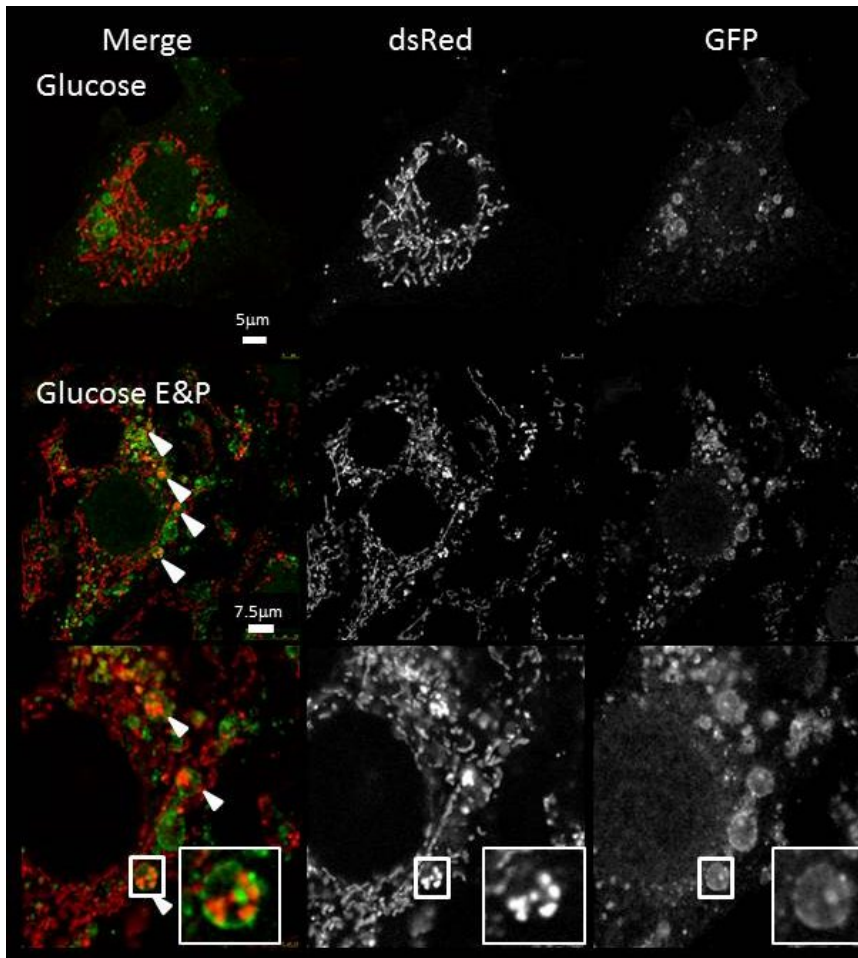
All animal studies were carried out with approval of the Local Ethical Review Panel at the University of Oxford under license in accordance with the UK Animals (Scientific Procedures) Act 1986.

Left panel: The number of LC3 positive puncta co-localising with mitochondrial signal at baseline and after Chloroquine (25 μ M chloroquine overnight) was decreased in Atg7 deficient mouse splenocytes (Atg7 KO, $P < 0.01$).

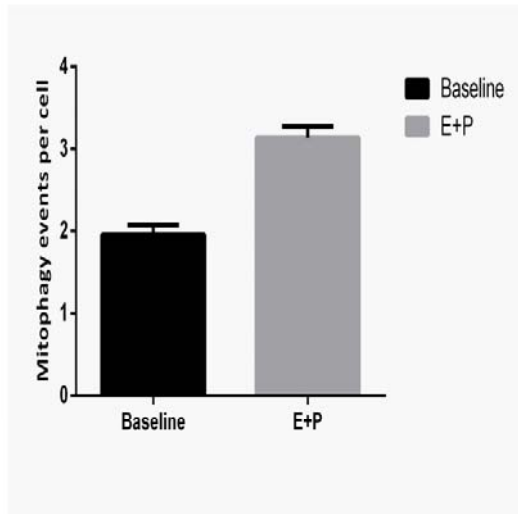
Right panel: Puncta that were both positive for LC3 and lysosomal marker, LysoID and co-localised with mitochondria were counted to estimate the effects of Atg7 knockdown on numbers of autolysosomes. These were reduced in splenocytes from the Atg7 knockout ($p < 0.01$). NB Chloroquine prevents lysosomal maturation by inhibiting acidification. Hence while it substantially increases the number of autophagosomes (ie of all LC3 positive puncta) co-localising with mitochondria (left) it does not much affect the counts of autolysosomes co-localising with mitochondria (right).

Figure e-2

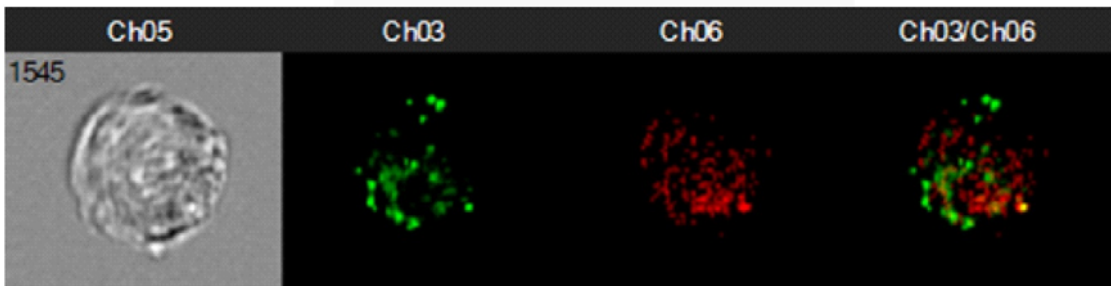
A)



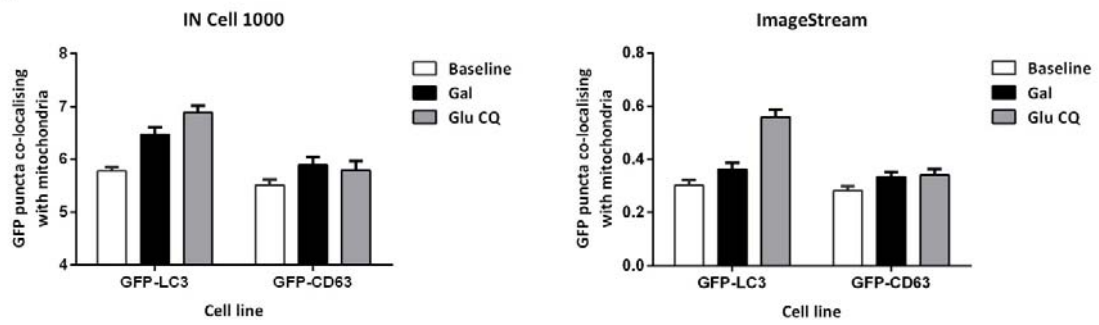
B



C



D



E

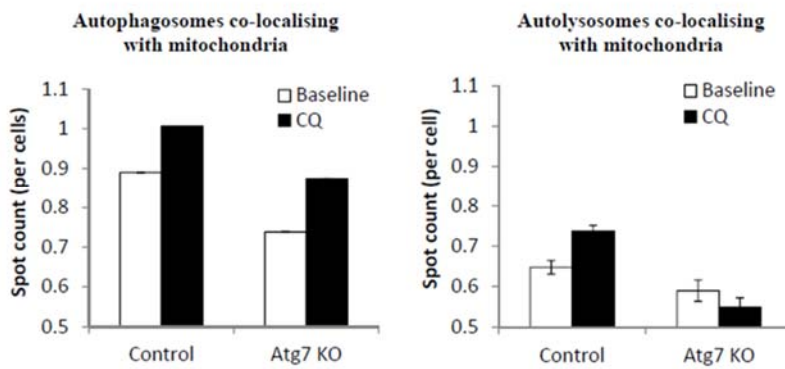


Figure e-3.**Addition cellular features of OPA1 knock down.**

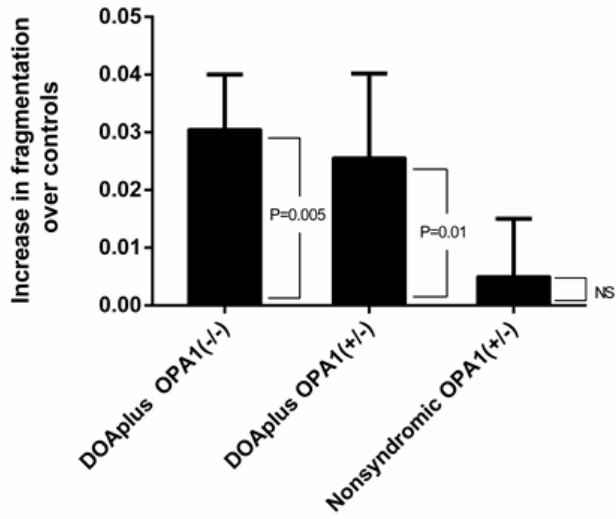
Figure e-3A Confirmation of increased mitochondrial fragmentation in bi-allelic patient fibroblasts using ImageStream output, aspect ratio (the minor axis divided by the major axis, describes how round or oblong an object is, being 1.0 for a circle and lower for elongated objects) of mitochondria was determined from ImageStream output (using a mitochondrial mask based on an intensity threshold of 30%, see methods). The difference between aspect ratio of each patient group and controls is shown as the Y axis in the chart. We show one bar per patient group, with each bar's height representing the estimated difference between a particular patient group and controls. The whiskers on a bar represent the standard error (SE) of the estimated difference (± 1 SE is shown); an approximate 95% confidence interval for the patient-control difference could be calculated as the bar height ± 2 SEs. The p-values in the figure are from the test of the null hypothesis that there is no actual difference between a patient group and controls. In eight experiments involving individuals listed in Table 1 and six controls, mitochondria in fibroblasts from bi-allelic and mono-allelic DOA plus patients are significantly more fragmented than mitochondria from controls ($p=0.005$ and 0.01 respectively). There was no significant difference between non-syndromic patients and controls.

Figure e-3B Microtubule dependence of the perinuclear mitochondrial clustering resulting from profound OPA1 knock down that was demonstrated in Figure 2: Dynein disruption by overexpression of p50-dynamitin-GFP rescues mitochondrial MTOC clustering due to loss of Opa1.

We hypothesized that clustering of mitochondria at the MTOC in KD cells may be due to either an imbalance of plus- and minus-end transport caused by excessive fragmentation and mitophagy or a hitherto unknown role of Opa1 in promoting plus-end directed transport of mitochondria. In either case, loss of Opa1 would cause a preponderance of negative-end-directed transport of mitochondria along microtubules towards the MTOC, leading to perinuclear clustering. Figure 2F illustrates how we tested this idea, by exposing cells to two microtubule-disrupting drugs: nocodazole and taxotere. Nocodazole causes the disassembly

of microtubules, whereas taxotere causes MTOC-independent, random assembly and stabilization of microtubules(7) that lack polarity and orientation(8). Treatment of Opa1 KD cells with nocodazole rescued the perinuclear clustering so that the distribution of mitochondria resembled that in control cells (Figure 2F(ii)). In contrast, taxotere treatment led to the formation of multiple, randomly distributed mitochondrial clusters. Finally, we also tested the role of actin filaments in Opa1 KD-mediated mitochondrial clustering by using the actin depolymerising drug cytochalasin D. As with nocodazole, treatment of KD cells with cytochalasin D caused a redistribution of mitochondria away from the MTOC, although weak perinuclear clustering was still observed in some cells. In all cases, treatment of scramble siRNA transfected cells with drugs had little effect on mitochondria (data not shown). These experiments confirm that the organization of MTOC and microtubules are pivotal to and upstream of the mitochondrial clustering caused by Opa1 KD. To determine which transport direction was involved we investigated the dynein/dynactin multi-protein complex(9) that mediates minus-end-directed transport of mitochondria. Overexpression of a GFP-tagged dynactin sub-unit (p50/dynamitin), disrupts the dynein/dynactin complex, leading to loss of minus-end transport(10, 11), which in turn is known to disrupt autophagy(12),(13). Mitochondrial clustering was apparent with TMRM staining of OPA1 siRNA treated cells transfected with pcDNA plasmid (control, lower panel), but not in those transfected with the p50 dynamitin GFP expressing plasmid (upper panel). Nuclei are marked by asterisks. This shows that clustering is rescued by p50 dynamitin GFP expression and therefore depends on minus-end microtubule transport. Mitochondrial distribution was not affected when the same transfections were carried out with scramble siRNA treatment.

A



B

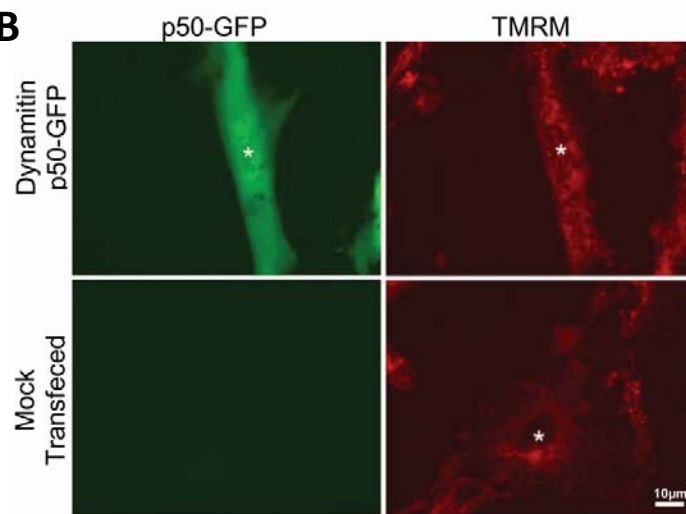


Figure e-4**e-4A Mitophagic flux is increased in fibroblasts of bi-allelic patients**

Co-localisation of mitochondria with LC3 positive puncta was quantified in fibroblasts from patient DOAplus OPA1(-/-)1 and two controls using IN Cell 1000 as above. Flux (defined as the increase in co-localisation relative to baseline) was greater in the patient than the controls ($p < 0.001$ at 24h) and increased appropriately over 24 hours.

e-4B Idebenone does not ameliorate the increased mitophagy in fibroblasts of bi-allelic patients

Co-localisation of mitochondria with LC3 positive puncta (expressed as mitophagy area as a percentage of mitochondrial area) in glucose-based media was not affected by 3 days exposure to idebenone 1uM for 72h (error bars are standard errors of technical replicates). This reflects idebenone treatment the animal model, in which there was no improvement (14).

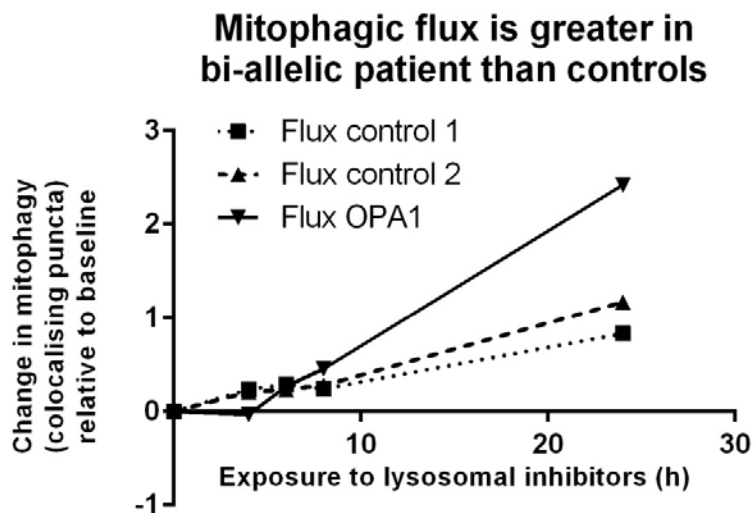
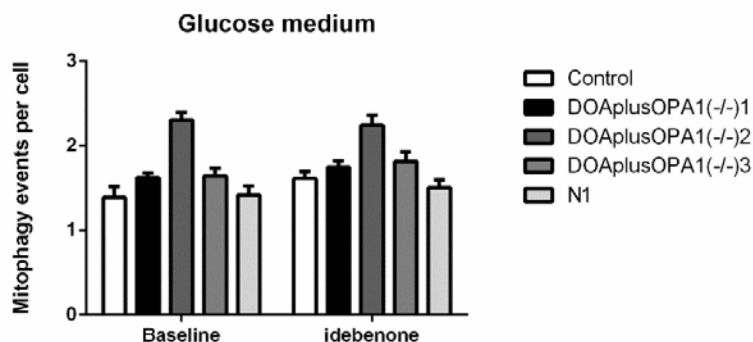
Figure e-4A**Figure e-4B**

Figure e-5 Western analysis of fibroblast protein

A Western blot analysis of OPA1, p62 and LC3 proteins relative to actin in *OPA1* mutant fibroblasts of patients DOAplus OPA1(-/-)1-3 and mitofusin 2 (MFN2) mutant fibroblasts compared to control. Cells were grown either in regular medium (Glu) or glucose-free galactose-based medium (Gal) for 48 hours.

B The abundance of summed OPA1 short and long isoforms (15) are reduced in the patients relative to the average control (Ave).

C LC3-II abundance (relative to actin) is increased in fibroblasts from patients DOAplusOPA1(-/-)2 and 3 but not DOAplusOPA1(-/-)1 compared to control

D Western blot analysis of OPA1 relative to GAPDH in *OPA1* mutant fibroblasts of patients DOAplus OPA1(+/-)1 and DOA OPA1(+/-) show a reduction in OPA1 abundance.

E Western blot analysis of OPA1 and LC3 proteins relative to actin in *OPA1* mutant fibroblasts of patient DOAplus OPA1(-/-)1 and his unaffected mother (N1) and unaffected grandfather (OPA1(+/-)1) compared to control. The lower OPA1 band correspond to the short (s-OPA1) and the upper two bands to the long (l-OPA1) isoforms (15). The levels of OPA1 both short and long forms are reduced in the patient and carrier grandfather relative to the control. LC3-I and LC3-II are increased in patient 1 but not his unaffected carrier grandfather compared to control.

Figure e-5.

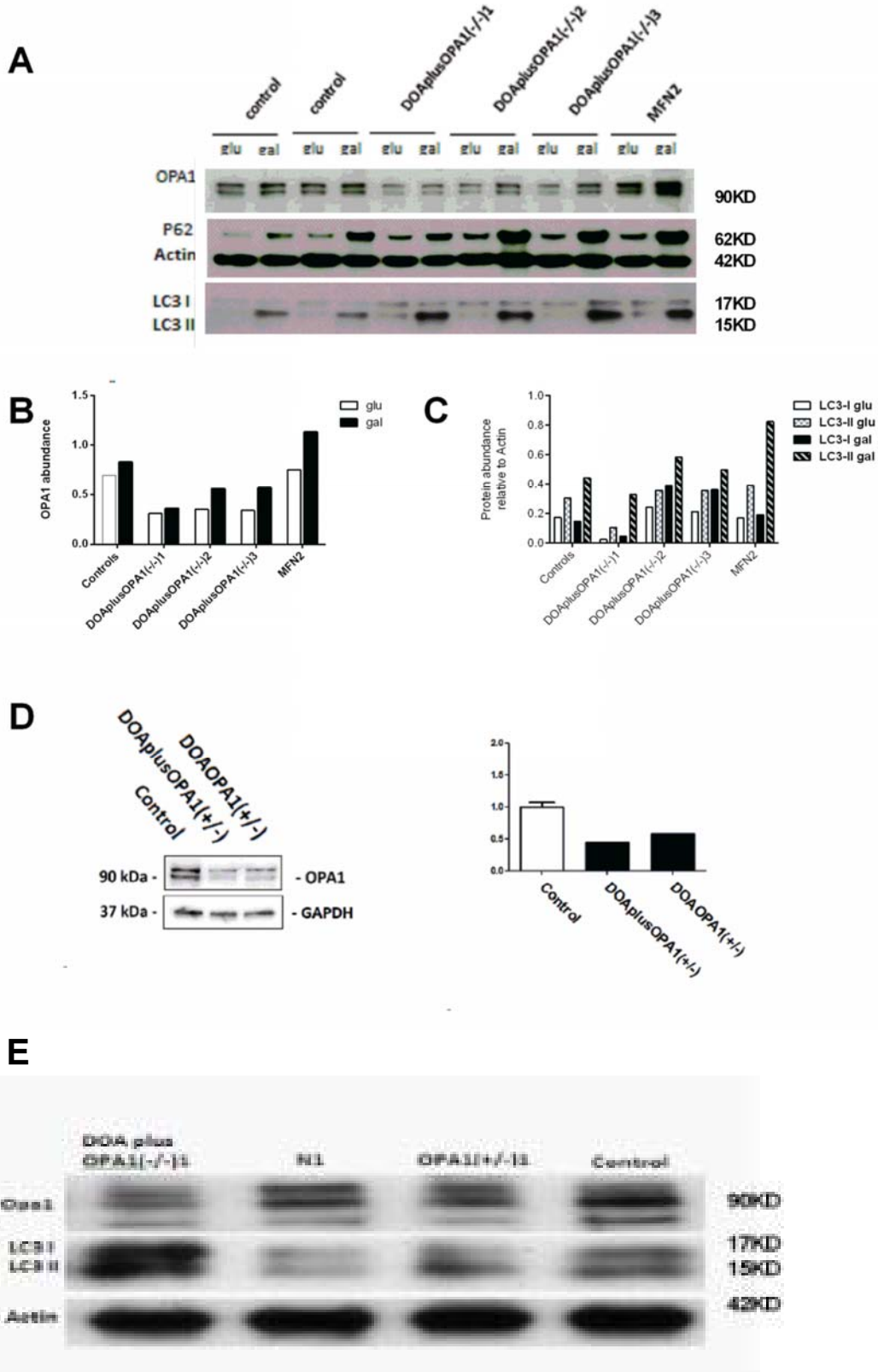


Figure e-6. OPA1 loss in fibroblasts leads to mitochondrial fragmentation without loss of cytochrome c or alteration of cristae.

a) Cytochrome c/Mitotracker red staining of fibroblasts treated with pan-*OPA1* or scrambled siRNA for 48 hours. There was no leakage of cytochrome c from mitochondria, [Bars 10 μ M]

b) Electron micrographs of mitochondria from control (left) and pan-*OPA1*/scrambled siRNA treated (right) fibroblasts showing the similar appearance of the mitochondrial cristae. [Bars 200 nm]. There was no gross increase in autophagosomes as seen by EM.

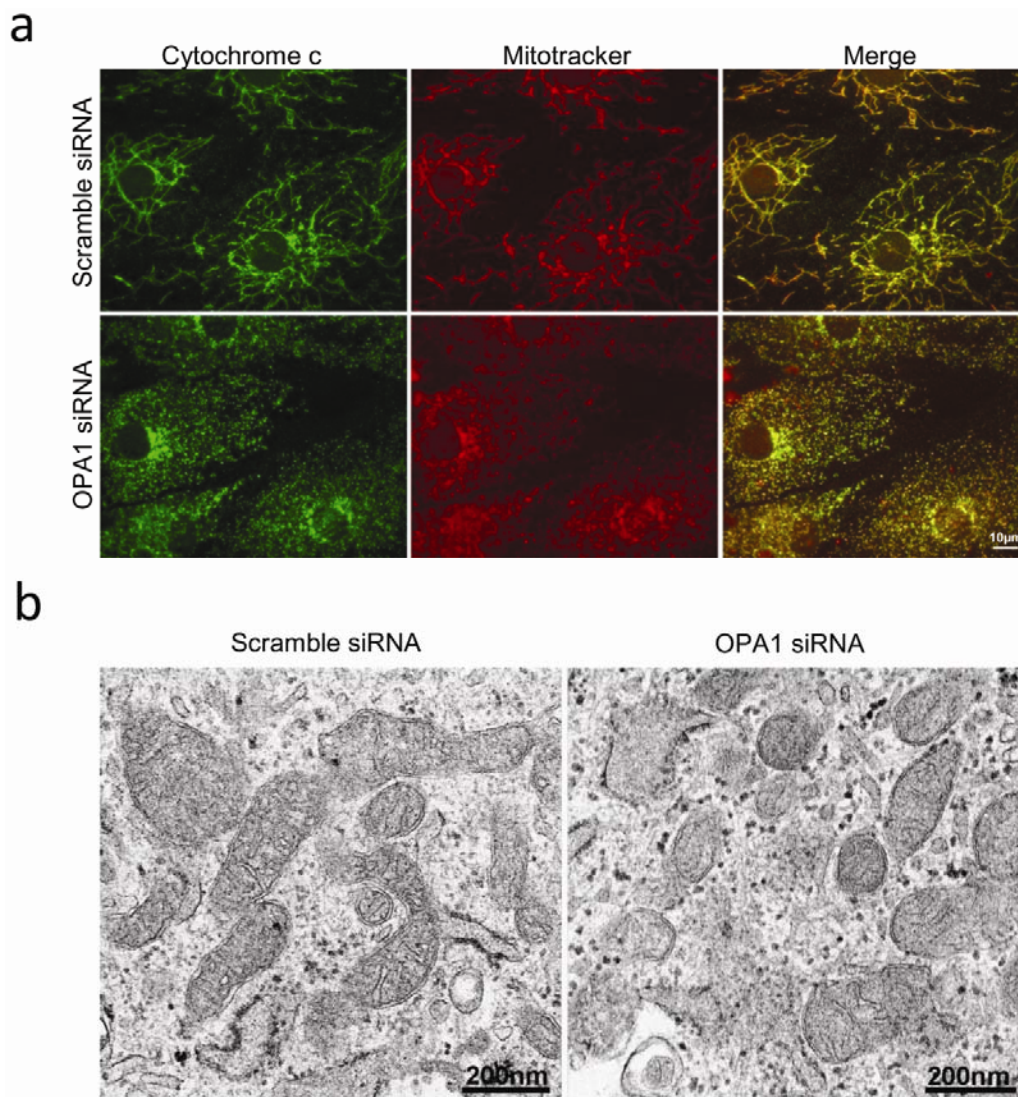
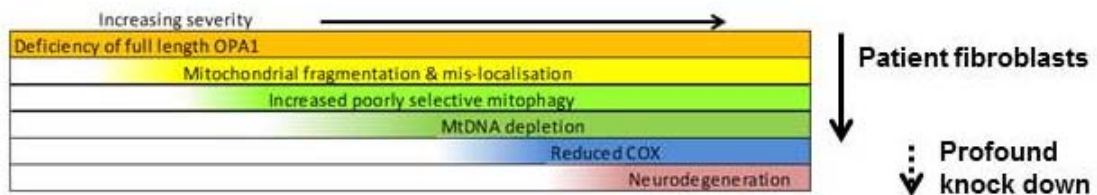


Figure e-7**Illustration of suggested sequence of events**

The diagram illustrates the sequence of events that may be occurring in affected tissue with increasingly severe depletion of full length OPA1. The first four stages are apparent in fibroblasts from patients. The portion indicated by the dotted arrow illustrates our postulate that mtDNA depletion causes significant mitochondrial dysfunction in some tissues, as is apparent in siRNA of control fibroblasts. That neurodegeneration is a direct consequence of this process is unproven.



Appendix e-2: Supplementary methods

Cell cultures (see Table 1)

Patient cultures

It is generally accepted that primary patient fibroblasts express both OPA1 protein deficiency(16) and defects in autophagy(17), and are hence appropriate for pathophysiological investigations. By characterising fibroblasts from four of the healthy or oligosymptomatic transmitting relatives of the three bi-allelic patients, we were able to study each of their *OPA1* mutations in mono-allelic cultures. Three DOA patients with dominantly inherited mutations in the *OPA1* GTPase domain were studied, of whom one had uncomplicated DOA, and two had DOA plus (DOA OPA1(+/-), DOAplusOPA1(+/-)1 and DOAplus OPA1(+/-)2 respectively, see Table 1).

Disease control culture

One fibroblast line from a patient with severe symptomatic dominantly inherited axonal Charcot-Marie-Tooth disease CMT2A2 due to the c.745T>A (p.Ser249Thr) in the large GTPase domain near the N-terminus of mitofusin 2 was used (MFN2).

Control cultures

Twenty anonymised control fibroblast cultures were used for comparison (designated “control” and not including unaffected family members whose designations are in Table 1), taken (i) with parental consent from children undergoing diagnostic skin biopsy for karyotyping or biochemical screen and where cytogenetics or similar was normal (n=2), and (ii) from healthy consented adults. The age range was thus 0-81 years. One control at the median mitophagic activity, whose age was within 3 years of patient DOAplus OPA1(-/-)1 was included in the vast majority of runs.

Cells with fluorescent organelles

To validate our methods we also used cultured cells with fluorescent mitochondria and autophagosomes or autolysosomes. These were HeLa cells expressing dsred targeted to mitochondria and GFP tagged either LC3 or the lysosomal marker CD63 (4) (courtesy of Aviva Tolkovsky). For comparison with a related defect in mitochondrial dynamics we also used cultures from a patient with MFN2 mutations.

Immunofluorescence and live cell imaging

Cells were processed for histochemistry(18), immunofluorescence or live staining with PicoGreen and TMRM as previously described(19). For fluorescence microscopy the antibodies used were: Anti-cytochrome c (Clone 6H2.B4, Biolegend); Anti-DNA IgM (Peter Cook); *OPA1* (Clone 18, BD Biosciences); Anti-pericentrin (ab4448, AbCam); and Anti-GM130 (clone EP892Y, AbCam). MtDNA staining in live cells was achieved by diluting stock PicoGreen solution at 3 μ l/ml (2 hours), then rinsed 3 times in pre-warmed PBS and mounted with phenol red free DMEM supplemented with 4.5g/l glucose and 25mM HEPES buffer, and visualised using a Leica DMI50 microscope. Mitochondrial co-labelling was achieved by incubating the cells in fresh medium containing 50nM Mitotracker red for 5 minutes before rinsing with fresh medium. Tetramethylrhodamine methyl ester (TMRM) staining was used to monitor mitochondrial membrane potential. Cells were incubated for 20 minutes in medium containing 50nM TMRM at 37°C and visualised without removal of the dye.

IN Cell 1000 high throughput imaging (20).

We previously validated IN Cell 1000 for detecting mitophagy (20). In brief, cells are cultured in a 96-well plate and treated for 6 hours in the indicated conditions before fixation with 4% paraformaldehyde (PFA). After DAPI and immuno-staining using a monoclonal antibody anti-TOM20 (Santa Cruz Biotechnology, mouse) and a polyclonal antibody anti-LC3 (Medical and Biological Laboratories, rabbit) combined to Alexa Fluor 488 Goat anti-rabbit and Alexa Fluor 568 Goat anti-mouse (life technologies) secondary antibodies the plate is imaged using the IN Cell1000 analyser (GE healthcare life sciences, 500 cells per well). Raw images were binarised and mitochondrial morphological characteristics were quantified, notably the degree of branching or mitochondrial form factor (FF) and the mean mitochondria length (in μ m).

Figures e-2A and e-2B show a comparison of IN Cell 1000 output with confocal microscopy, using mouse embryonic fibroblasts in which dsred is targetted to mitochondria and GFP to autophagosomes by tagging LC3. Exposure to lysosomal inhibitors E64d and Pepstatin A increases the co-localisation of mitochondria with autophagosomes by both techniques, microscopy showing that the mitochondrial fragments are engulfed.

ImageStream validation for analysis of mitophagy

We also used ImageStream (Amnis) to quantify mitophagy in fibroblast cultures from patients and controls. This was previously validated as a method for detecting autophagy (21)

Primary cell cultures were harvested, washed in PBS, and fixed with 4% paraformaldehyde for 15 minutes at room temperature and permeabilized by adding 0.4% triton to the fixative for 5 minutes. They were then immunostained with antibodies to the E1 α subunit of PDH (Mitoscience) or LC3 (Cell Signalling Technology) followed by anti-mouse Alexa-488 and anti-rabbit Alexa-546 secondary antibodies respectively (Invitrogen), counting 1000-5000 cells in each condition on each of three occasions. An example of raw output from ImageStream is shown in Figure e-2C.

To identify co-localisation of autophagosomes and mitochondria as an indicator of mitophagy we used Amnis IDEAS software. Initially we quantitated bright detail similarity (BDS) of mitochondrial and LC3 signals. BDS is a feature that calculates the degree of overlapping pixel intensities taken from different channels of fluorescent imagery and is the log-transformed Pearson's correlation coefficient that is non mean normalized. It is applied either to the open residue image or to a masked image designed to detect LC3 puncta (spots of ~ 1 μm with an LC3 intensity that contrasted with the rest of the cell by more than 3-6 fold basal intensity). However, we found that counting the numbers of LC3/LysoID positive puncta was more robust than using BDS, especially in runs with a relatively high background. As well as the total number of such spots per cell, we compared the number of LC3/lysoID positive puncta that co-localized with mitochondria, using a "threshold" mask detecting mitochondrial location. The threshold mask is used to exclude pixels, based on a percentage of the range of intensity values as defined by the starting mask. We routinely counted the numbers of LC3 puncta co-localising with the mitochondrial signal, defined by using thresholds at both 30% and 70% of the mitochondrial signal intensity. For these features to be accurate, it is essential to gate on cells that are bright for both fluorescent markers of interest (double positive population).

We used ImageStream for a small proportion of our experiments as we found that IN Cell 1000 was superior in its resolution, cost and reliability. Figure e-2D shows that the output of this method correlates closely with that of IN Cell 1000, which we had validated for detecting mitophagy(20). We further validated ImageStream for detecting mitophagy by knocking down the essential autophagy protein, Atg7 in mouse splenocytes (Figure e-2E).

ImageStream and IN Cell 1000 shares a significant advantage over older methods for detecting both autophagy and mitophagy: both are high throughput techniques that are both objective and quantitative (figure e-2 compares them with confocal microscopy). However, we were unable to detect PINK or Parkin signal using either method, nor could we follow single autophagosome events in real time. To our knowledge ImageStream has not previously been used to investigate mitophagy in detail.

Quantifying form factor and autophagic flux with ImageStream and IN Cell 1000

FF is defined as $(Pm^2)/(4\pi Am)$, where Pm is the length of mitochondrial outline and Am is the area of mitochondrion(22), and with a value comprised between 1 (fragmented network in individual dots) and 0 (infinitely connected network). Mitochondria with a FF >0.8 are fragmented and their proportion is calculated among all the mitochondria identified. For ImageStream output this was determined from output using a threshold of 30% for intensity of PDH signal.

In order to detect the autophagic flux, we used the lysosomal protease inhibitors pepstatin A and E64D, or chloroquine that blocks lysosomal acidification (either 25 μ M overnight or 10-100 μ M for 2 hours). Autophagy inducing protocols were starvation (minimal media for 2 hours), or culture in galactose-based media lacking glucose for 12-72 hours.(23, 24). Autophagic flux was defined as the difference between lysosomal inhibitors added and no lysosomal inhibitors added (basal levels) relative to basal levels(24). So we defined mitophagic flux similarly, as the difference between mitophagy with lysosomal inhibitors added and no lysosomal inhibitors added (basal levels) relative to basal levels in mitophagy with inhibitors minus without inhibitors over basal levels (Figure 3D and figure e-2E).

Figure e-2D illustrates ImageStream output from primary cells stained for LC3 and pyruvate dehydrogenase. Starvation (either minimal or galactose medium) or the presence of lysosomal inhibitors reproducibly increased co-localisation of mitochondrial signal with LC3 puncta (Figure 3A shows patient and age-matched control in galactose medium).

Chloroquine inhibits autophagy and hence reproducibly increased the number of LC3 puncta per cell as well as bright detail similarity (BDS, a score of the co-localisation of two markers in puncta where mitochondrial and LC3 signal co-localised), co-localised spot intensity and

co-localised spot count (Figure 3B, $p < 0.001$). Furthermore it could be inhibited knock down of autophagy protein ATG7 (figure e-3A).

Western blotting

2×10^5 cells were seeded in the plate and grown at 37°C overnight. Cells were washed twice in cold PBS and harvested in 50ul 1X Laemmli sample buffer. The cells were then lysed by pulsing the sonicator for 5 seconds on/5 seconds off, twice, heated at 95°C for 5mins, and centrifuged at 15700g for 1 minute. 10ul of the supernatant were loaded on to a 4-20% gel for SDS-PAGE. Protein was separated by electrophoresis at 125V for 2 hours (Figure 3). The LC3 antibody was from MBL International Corporation (Cat. No: PM036). The OPA1 antibody was from BD transduction laboratories (Cat. No: 612606). The P62 antibody is from BD transduction laboratories (Cat.No: 610832). The actin antibody is from cell signalling (Cat. No: 11/2011).

Electron Microscopy

The cell pellets were fixed in 2.5 % glutaraldehyde in 0.1M phosphate buffer, post-fixed in osmium tetroxide, dehydrated and embedded in epoxy resin. Thin sections were cut and stained with uranyl acetate and lead citrate prior to examination in a Jeol 1200EX electron microscope.

RNAi and Plasmid Transfections

RNAi for *OPA1* was carried out as previously (25) using 50nM siRNA control and target Dharmacon 1 transfection agent (Thermo-Fisher). The *ATG7* siRNA used SMARTpool: ON-TARGETplus from Thermo scientific, Cat: L-020112-00-0005, Scramble siRNA: siGENOME Non-Targeting, Thermo scientific, Cat:# D-001210-02-05A.

Statistical Analysis

ImageStream output (such as the mean number of LC3 puncta co-localising with mitochondria, the number of cells and standard deviation) from eight experiments involving individuals listed in Table 1 and five controls was analysed using R version 2.15.2 (the R Foundation for Statistical Computing). The components of the regression equation were: Patient ID, run ID and patient group. Separate analyses were run by grouping patients in different ways, and for each analysis each patient group was compared to the controls. In

this way we determined the relationship between genotype and cellular phenotype of the patient cultures in the presence or absence of chloroquine.

Figures 1D and 2C contain one bar per patient group, with each bar's height representing the estimated difference between a particular patient group and controls. The whiskers on a bar represent the standard error (SE) of the estimated difference (± 1 SE is shown); an approximate 95% confidence interval for the patient-control difference could be calculated as the bar height ± 2 SEs.

The p-values in the figure are from the test of the null hypothesis that there is no actual difference between a patient group and controls. Useful intuition connecting the hypothesis test with the estimated difference is that a p-value < 0.05 corresponds to a 95% confidence interval not overlapping zero.

References

1. Chapman T, Hadley G, Fratter C, Cullen S, Bax B, Bain M, et al. Unexplained gastrointestinal symptoms: Think mitochondrial disease. *Digestive and Liver Disease*. 2013; 46 (1): 1-8.
2. Toomes C, Marchbank NJ, Mackey DA, Craig JE, Newbury-Ecob RA, Bennett CP, et al. Spectrum, frequency and penetrance of OPA1 mutations in dominant optic atrophy. *Hum Mol Genet*. 2001;10(13):1369-78.
3. Nochez Y, Arsene S, Gueguen N, Chevrollier A, Ferre M, Guillet V, et al. Acute and late-onset optic atrophy due to a novel OPA1 mutation leading to a mitochondrial coupling defect. *Mol Vis*. 2009;15:598-608.
4. Bampton ET, Goemans CG, Niranjan D, Mizushima N, Tolkovsky AM. The dynamics of autophagy visualized in live cells: from autophagosome formation to fusion with endo/lysosomes. *Autophagy*. 2005;1(1):23-36.
5. Mortensen M, Ferguson DJ, Edelmann M, Kessler B, Morten KJ, Komatsu M, et al. Loss of autophagy in erythroid cells leads to defective removal of mitochondria and severe anemia in vivo. *Proc Natl Acad Sci U S A*. 2010;107(2):832-7.
6. Mortensen M, Soilleux EJ, Djordjevic G, Tripp R, Lutteropp M, Sadighi-Akha E, et al. The autophagy protein Atg7 is essential for hematopoietic stem cell maintenance. *J Exp Med*. 2011;208(3):455-67.
7. Jordan MA, Wilson L. Use of drugs to study role of microtubule assembly dynamics in living cells. *Methods Enzymol*. 1998;298:252-76.
8. McNiven MA, Porter KR. Microtubule polarity confers direction to pigment transport in chromatophores. *J Cell Biol*. 1986;103(4):1547-55.
9. Vallee RB, Okamoto PM. The regulation of endocytosis: identifying dynamin's binding partners. *Trends Cell Biol*. 1995;5(2):43-7.
10. Burkhardt JK, Echeverri CJ, Nilsson T, Vallee RB. Overexpression of the dynamin (p50) subunit of the dynactin complex disrupts dynein-dependent maintenance of membrane organelle distribution. *J Cell Biol*. 1997;139(2):469-84.

11. Varadi A, Johnson-Cadwell LI, Cirulli V, Yoon Y, Allan VJ, Rutter GA. Cytoplasmic dynein regulates the subcellular distribution of mitochondria by controlling the recruitment of the fission factor dynamin-related protein-1. *J Cell Sci.* 2004;117(Pt 19):4389-400.
12. Yamamoto M, Suzuki SO, Himeno M. The effects of dynein inhibition on the autophagic pathway in glioma cells. *Neuropathology.* 2010;30(1):1-6.
13. Maday S, Wallace KE, Holzbaur EL. Autophagosomes initiate distally and mature during transport toward the cell soma in primary neurons. *J Cell Biol.* 2012;196(4):407-17.
14. Smith TG, Seto S, Ganne P, Votruba M. A randomized, placebo-controlled trial of the benzoquinone idebenone in a mouse model of OPA1-related dominant optic atrophy reveals a limited therapeutic effect on retinal ganglion cell dendropathy and visual function. *Neuroscience.* 2016;319:92-106.
15. Satoh M, Hamamoto T, Seo N, Kagawa Y, Endo H. Differential sublocalization of the dynamin-related protein OPA1 isoforms in mitochondria. *Biochem Biophys Res Commun.* 2003;300(2):482-93.
16. Amati-Bonneau P, Milea D, Bonneau D, Chevrollier A, Ferre M, Guillet V, et al. OPA1-associated disorders: phenotypes and pathophysiology. *Int J Biochem Cell Biol.* 2009;41(10):1855-65.
17. Cullup T, Kho AL, Dionisi-Vici C, Brandmeier B, Smith F, Urry Z, et al. Recessive mutations in EPG5 cause Vici syndrome, a multisystem disorder with defective autophagy. *Nat Genet.* 2013;45(1):83-7.
18. Elson JL, Samuels DC, Johnson MA, Turnbull DM, Chinnery PF. The length of cytochrome c oxidase-negative segments in muscle fibres in patients with mtDNA myopathy. *Neuromuscul Disord.* 2002;12(9):858-64.
19. Ashley N, Harris D, Poulton J. Detection of Mitochondrial DNA Depletion in Living Human Cells using PicoGreen Staining. *Experimental Cell Research.* 2005;303:432-46.
20. Diot A, Hinks-Roberts A, Lodge T, Liao C, Dombi E, Morten K, et al. A novel quantitative assay of mitophagy: combining high content analysis fluorescence with mitochondrial DNA mutant load to identify novel pharmacological modulators of mitophagy. *Pharmacological Research.* 2015;100:24-35.
21. Phadwal K, Alegre-Abarrategui J, Watson AS, Pike L, Anbalagan S, Hammond EM, et al. A novel method for autophagy detection in primary cells: Impaired levels of macroautophagy in immunosenescent T cells. *Autophagy.* 2012;8(4).
22. Mortiboys H, Thomas KJ, Koopman WJ, Klaffke S, Abou-Sleiman P, Olpin S, et al. Mitochondrial function and morphology are impaired in parkin-mutant fibroblasts. *Ann Neurol.* 2008;64(5):555-65.
23. Schmid D, Pypaert M, Munz C. Antigen-loading compartments for major histocompatibility complex class II molecules continuously receive input from autophagosomes. *Immunity.* 2007;26(1):79-92.
24. Klionsky DJ, Baehrecke EH, Brumell JH, Chu CT, Codogno P, Cuervo AM, et al. A comprehensive glossary of autophagy-related molecules and processes (2nd edition). *Autophagy.* 2011;7(11):1273-94.
25. Ashley N, Poulton J. Anticancer DNA intercalators cause p53-dependent mitochondrial DNA nucleoid re-modelling. *Oncogene.* 2009;28(44):3880-91.